The Glass Transition Temperature (T_g) as an Index of Chemical Conversion for a High-T_g Amine/Epoxy System: Chemical and Diffusion-Controlled Reaction Kinetics

G. WISANRAKKIT and J. K. GILLHAM, *Polymer Materials Program, Department of Chemical Engineering, Princeton University, Princeton, NJ 08544-5263*

Synopsis

The glass transition temperature (T_g) is used as a parameter to monitor the isothermal cure of a tetrafunctional aromatic diamine and a difunctional aromatic epoxy system. There is a one-to-one relationship between T_g and conversion that is independent of cure temperature, T_{cure}. Prior to vitrification ($T_g = T_{cure}$), the reaction is only kinetically controlled; after vitrification, the reaction becomes diffusion-controlled. Time-temperature shifts of T_g vs. ln(time) data at different cure temperatures to form a master curve for the kinetically controlled reaction at an arbitrary reference temperature yield a single Arrhenius activation energy (15.2 kcal/mole). The master curve and the reaction activation energy are used in calculating iso-T_g contours prior to vitrification and also the vitrification contour in the time-temperature-transformation (TTT) isothermal cure diagram for the system. The chemical kinetics of the reaction is satisfactorily described by an autocatalyzed reaction mechanism. The overall rate constant of the reaction in both kinetically and diffusion-controlled regimes is modeled by a combination, in parallel, of the chemical rate constant and the diffusion rate constant. The chemical rate constant has the usual Arrhenius form, whereas the diffusion rate constant is assumed to be given by a modified form of the WLF equation. Results suggest that both primary and secondary amino hydrogens are equally reactive. A theoretical model for calculating T_g as a function of conversion is presented for a network-forming system with one bond-forming reaction.

INTRODUCTION

Curing of thermosetting materials generally involves the transformation of low molecular weight liquids to high molecular weight amorphous solids by means of chemical reactions. The curing process is of particular importance in the making of structural composites, coatings, adhesives, and electronic encapsulants. A useful framework for understanding and conceptualizing the changes that occur during cure of a thermosetting system is the isothermal time-temperature-transformation (TTT) cures. Such a diagram, schematically shown in Figure 1, displays the states of the material and characterizes the changes in the material during isothermal cure vs. time.[1-3] Material states include liquid, sol glass, sol/gel rubber, gel rubber, sol/gel glass, gel glass, and char. The various changes occurring in the material during isothermal cure are characterized by contours of the times to reach the events. Relevant contours could include molecular gelation (corresponding, for the simplest systems, to the unique conversion at the molecular gel point), macroscopic gelation (not

WISANRAKKIT AND GILLHAM
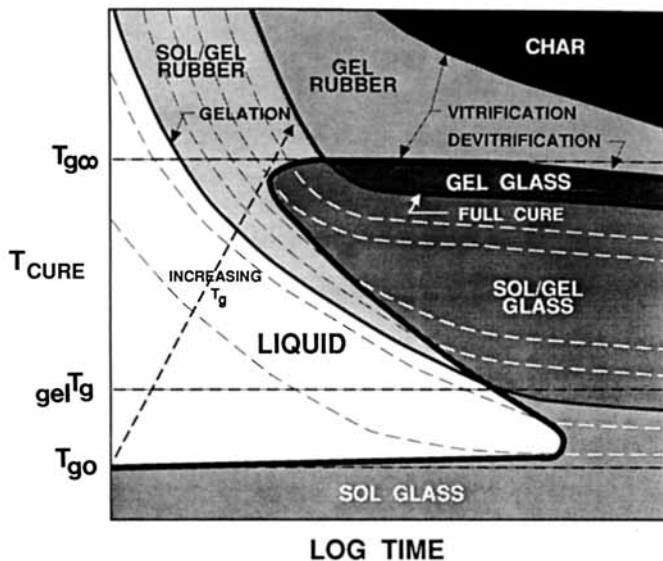
TTT CURE DIAGRAM

Fig. 1. A generalized isothermal time-temperature-transformation (TTT) cure diagram for a thermosetting system, showing three critical temperatures (i.e., T_{g0}, $T_{g\infty}$, and $_{gel}T_g$), states of the material, and contours characterizing the setting and degradation processes. The full cure contour corresponds to $T_g = T_{g\infty}$. Molecular gelation corresponds to $T_g = {}_{gel}T_g$. Other iso-T_g contours are included (dashed lines).

shown in Fig. 1) (corresponding, e.g., to an iso-viscosity state), vitrification (corresponding to the glass transition temperature, T_g, rising to the cure temperature, T_{cure}), devitrification (corresponding to T_g decreasing to T_{cure} because of thermal degradation), and char formation (corresponding to T_g increasing to T_{cure} because of thermal degradation). The progress of the isothermal cure process and the state of the material can be clearly summarized in terms of these contours in the TTT diagram. Three critical temperatures are marked on the temperature axis of Figure 1: T_{g0}, the glass transition temperature of the uncured reactants, $_{gel}T_g$, the temperature at which molecular gelation and vitrification coincide, and $T_{g\infty}$, the glass transition temperature of the fully cured network.

The basic parameter governing the state of the material is the chemical conversion. Therefore, knowledge of the kinetic rate of curing and how the rate changes with cure temperature is important and useful for predicting the chemical conversion achieved after a cure schedule. However, the chemical kinetics of most thermosets at cure temperatures below $T_{g\infty}$ is generally complicated by the fact that the reactions become diffusion-controlled in the later stages of cure, particularly after vitrification,[4,5] where the rates of the chemical reactions become very low. Complete kinetic characterization over the wide ranges of time and temperature of cure using conventional parameters to monitor the chemical conversion of the materials, such as infrared absorption bands of

reactants and products, and heats of reaction, are not always successful because these parameters are often not sensitive to small changes in chemical conversion, especially at high conversion and in diffusion-controlled regimes.

A parameter that shows considerable increase accompanying the changes in chemical conversion during cure of a themosetting material is the glass transition temperature, T_g. The fact that T_g increases nonlinearly with conversion in crosslinking systems makes it more sensitive in the later stages of cure. As already mentioned, sensitivity is needed when the reaction rate is low, for example, at high conversion and after vitrification. Moreover, T_g can be measured accurately and easily throughout the entire range of cure. The combination of these facts suggests that T_g can be a sensitive and practical parameter for following the cure process of reactive thermosetting systems.

In this report, T_g is developed as an index of chemical conversion for a model study of an amine-cured epoxy system. Differential scanning calorimetry (DSC) is used to relate T_g data to chemical conversion. The reaction kinetics of the system in both kinetically and diffusion-controlled regimes is analyzed using the T_g data converted to a conversion basis. Both experimental data and a theoretical model of T_g vs. conversion are presented to support the premise that there is a direct one-to-one relationship between T_g (as measured) and chemical conversion.

A shorter version of this manuscript has been published.[6] A more complete report can be found in Ref. 7.

CHEMICAL SYSTEM

The chemical system chosen for this study is a diglycidyl ether of bisphenol A (DER332, Dow Chemical Co.) cured with a stoichiometric amount of a tetrafunctional aromatic diamine, trimethylene glycol di-p-aminobenzoate (TMAB: Polarcure 740M, Polaroid Corp). The chemical structures of both reactants are included in Fig. 2. The epoxy monomer is a viscous liquid with an epoxide equivalent weight (EEW) of 174 g/eq (determined by bromine titration by Dow Chemical Co., cf. EEW = 170 g/eq for the pure chemical). The amine curing agent is a highly crystalline solid (melting point = 125°C) with an amine equivalent weight of 157 g/eq.

Mixing Procedure

The crystalline amine was dissolved in the liquid epoxy monomer at 100°C. Complete dissolution took place within 15 min with vigorous stirring. This procedure was adopted in order to ensure homogeneous mixing and to avoid the use of solvent, the presence of which could complicate analysis of the reaction kinetics. Immediately after mixing, the warm liquid was degassed under vacuum at room temperature (RT) for 10 min. The resulting clear viscous liquid mixture was poured into numerous aluminum weighing pans, which were individually sealed in plastic bags, kept inside a dessicator, and stored in the freezer part of a refrigerator (the ambient temperature of which is approximately −15°C). For the kinetic study of this report, the conversion during mixing is neglected. The initial conversion after mixing was determined to be less than 1% (by

CHEMICAL REACTANTS
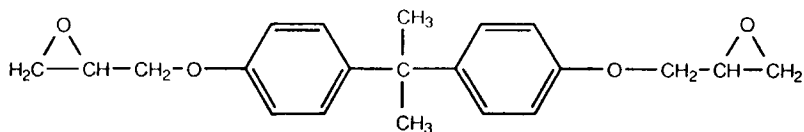
Diglycidyl Ether of Bis-phenol A (DER332, Dow Chemical Co.)
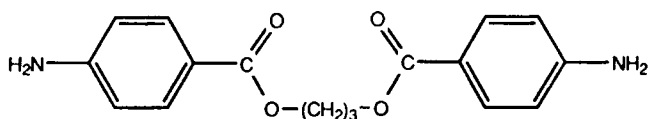
Trimethylene glycol di-p-aminobenzoate (TMAB, Polaroid Corp.)

REACTIONS

(1) $R-NH_2$ + (epoxide) $\longrightarrow$ (product)

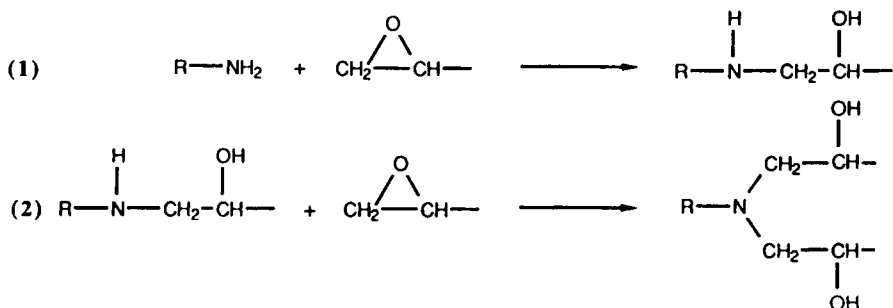(2) $R-N(H)-CH_2-CH(OH)-$ + (epoxide) $\longrightarrow$ (product)

Fig. 2. Chemical reactants and reactions.

chemical titration performed by Dow Chemical Co. and by calculation from the reaction kinetics developed during the course of this work).

EXPERIMENTAL PROCEDURE

All experiments in this study were performed using differential scanning calorimetry (DSC). A Perkin-Elmer instrument (DSC-4) was used to measure the T_g and the residual exotherm, ΔH_r, of the reaction after the material had been subjected to isothermal curing for prespecified times.

The initial reactive mixture, inside its plastic bag, was removed from the refrigerator and allowed at least 20 min to reach room temperature before being taken out of the plastic bag (to prevent moisture condensation onto the surface of the cold material). A small amount of the reactive mixture (approx. 10–20 mg) was transferred into a small DSC aluminum pan, which was subsequently sealed with an aluminum lid (by crimping around the edge). Sealed samples

were cured inside the DSC instrument isothermally under continuous N_2 flow for prespecified times. Isothermal curing was carried out at six different temperatures (100, 120, 140, 150, 160, and 180°C). After curing times ranging from 10 min to 24 h, each specimen was quenched from T_{cure} to −30°C at a programmed rate of 320°C/min and then subjected to a temperature scan from −30 to 370°C at 10°C/min to determine the T_g of the material after cure and the residual exotherm, ΔH_r, of the remaining reaction. A typical DSC scan is shown in Figure 3.

Experiments were also performed for cure times greater than 24 h. However, in these cases, samples, sealed in DSC aluminum pans, were cured together isothermally in a press oven under continuous N_2 flow. A specimen was removed from the press oven each day (up to 1 week), freely quenched from oven to room temperature, immediately transferred to the DSC unit at 30°C, quenched to −30°C (at 320°C/min), and then rescanned in the DSC unit from −30 to 370°C at 10°C/min. The T_g and the residual exotherm results of samples cured in the oven for 24 h were very close to those of samples cured at the same isothermal temperature in the DSC unit for 24 h. Thus, this procedure did not introduce significant error that might have arisen from a temperature mismatch between the press oven and the DSC unit. Periodic opening of the curing oven to remove specimens introduced only negligible fluctuations in the integrated cure histories for the remaining specimens, which were cured for longer times,
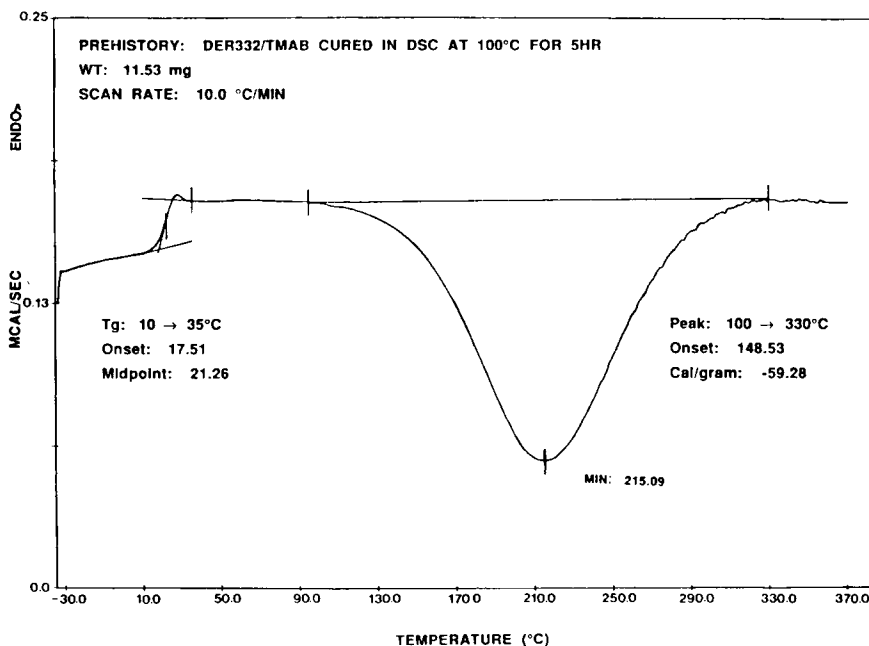

Fig. 3.   A typical DSC scan (heat flow vs. temperature) of a partially cured sample. The glass transition appears as a endothermic shift in the heat flow over a temperature interval. In this work, T_g is defined as the midpoint of the step-transition. The residual heat of reaction of the remaining reactants (ΔH_r) appears as an exothermic peak in the temperature region of the rubbery state of the material.

since the time needed for removing a sample ($\sim$ 1 min) was insignificant in comparison with the cure times ($\geq$ 24 h).

Samples that had vitrified ($T_g \geq T_{cure}$) for prolonged cure times underwent sub-T_g physical annealing at the temperature of cure. On the first DSC scanning up (from $-30°C$) through T_g, these samples exhibited a large endothermic peak in the glass transition interval. These specimens were quickly quenched (at a programmed rate of $320°C/min$) from temperatures just above the endothermic peaks to $-30°C$ and were then immediately reheated from -30 to $370°C$ at $10°C/min$. This procedure was necessary in order to eliminate the endothermic annealing peaks, the presence of which could complicate the assignments of T_g. Figure 4 shows typical DSC scans of one of these specimens. The short heating scans from $-30°C$ (at $10°C/min$) to beyond the endothermic peaks did not introduce significant change in the estimate of the chemical conversion of the sample as the glass transition temperature intervals of the first and second scans were virtually the same.

T_g appears as an endothermic shift over a temperature interval in the DSC scan. In this study, T_g was taken as the midpoint of the step-transition (see Fig. 3). The residual exotherm of the remaining reactants (ΔH_r) appears as an exothermic peak in the temperature range of the rubbery state of the material. The heat of reaction is estimated by drawing a straight line connecting the base line before and after the peak and integrating the area under the peak. The total heat of reaction ($\Delta H_T = 90$ cal/g, or 27.81 Kcal/mol of epoxide) was determined in the same way by scanning an initial (uncured) sample. The fractional conversion x was quantitatively calculated as[8]

$$x = 1 - \frac{\Delta H_r}{\Delta H_T} \tag{1}$$

RESULTS AND DISCUSSION

Experimental T_g vs. Residual Heat of Reaction

The progress of T_g and the corresponding residual heat of reaction, ΔH_r, of the material cured at $160°C$ for different times are shown in Figure 5. Both T_g and ΔH_r change monotonically with cure time; T_g increases while ΔH_r decreases until the reactants are fully depleted. The residual exotherm is used directly to calculate the extent of reaction according to eq. (1). It can be seen in Figure 5 that, although in the later stages of cure T_g shows noticable increase, the residual exotherm is almost unmeasurable in the DSC scan. When the heat content changes are low, the determination of T_g is more accurate than the measurement of ΔH_r since the relevant temperature interval involved is much narrower. T_g is taken as the midpoint of the endothermic step-change in the DSC scan over the temperature range of the glass transition ($\sim$ 40°C), whereas the residual heat of reaction, which becomes very small and difficult to determine accurately at high conversion, is measured from the exothermic peak over a wider temperature interval (up to approximately 200°C) in the rubbery state of the material.

Figure 6 shows the residual exotherm vs. T_g plotted for different cure temperatures (100, 120, 140, 150, 160, and 180°C). The results for each cure temperature cover a wide range of T_g and clearly overlap those for other cure temperatures. It is apparent for this epoxy/amine system that there is a unique one-to-one relationship, independent of cure temperature, between T_g and the residual exotherm and, therefore, between T_g and conversion. The results at high conversion (high T_g) are more scattered. This is attributed to the errors involved in the determination of the low residual exotherms at high conversions that tend to be underestimated due to the inadequate sensitivity of the DSC technique to low reaction rates. (Analysis of the high conversion data to obtain the residual exotherms involved the use of expanded DSC scales.)

The data in Figure 6 (excluding those that were clearly underestimated) are fitted with a third-order polynomial shown by the solid curve in the figure. The correlation of the fit is .998. The same data are also plotted in Figure 7 as T_g vs. fractional conversion. In the following analyses and discussions, T_g will be treated as a direct measure of the extent of reaction, and when desired, the results are converted to the corresponding conversion through this fitting polynomial.

Time-Temperature Shift of T_g vs. Time

The variation of T_g with cure time for the six isothermal cure temperatures is shown in Figure 8. Isothermal vitrification points ($T_g = T_{cure}$) for the cure
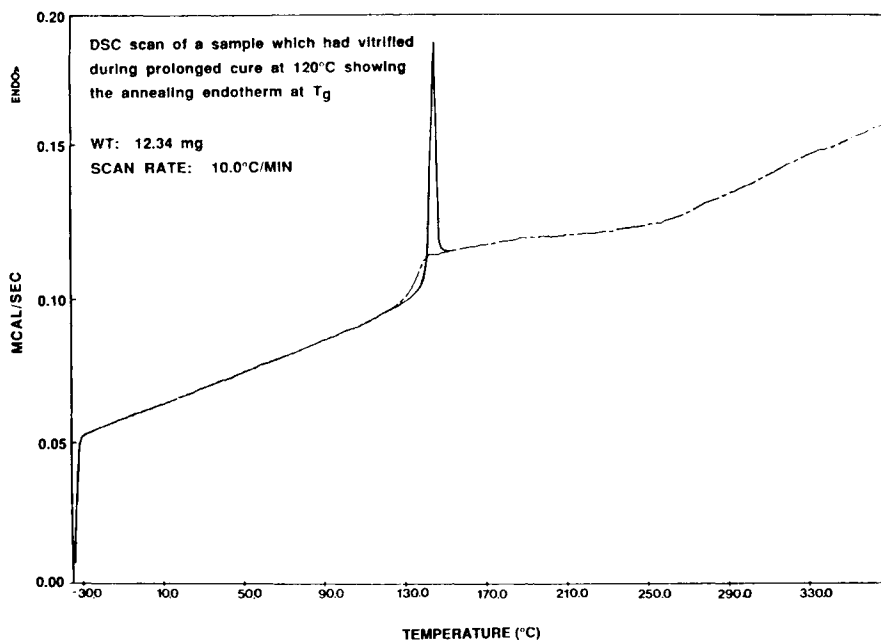

Fig. 4. Typical DSC scans of a partially cured sample that had vitrified during prolonged isothermal cure: (solid line) the first temperature scan of the sample (after quenching from the cure temperature to −30°C) from −30°C to a temperature just beyond the endothermic peak; (dashed line) the second temperature scan from −30 to 370°C of the same sample after quenching from a temperature immediately above the endothermic annealing peak.
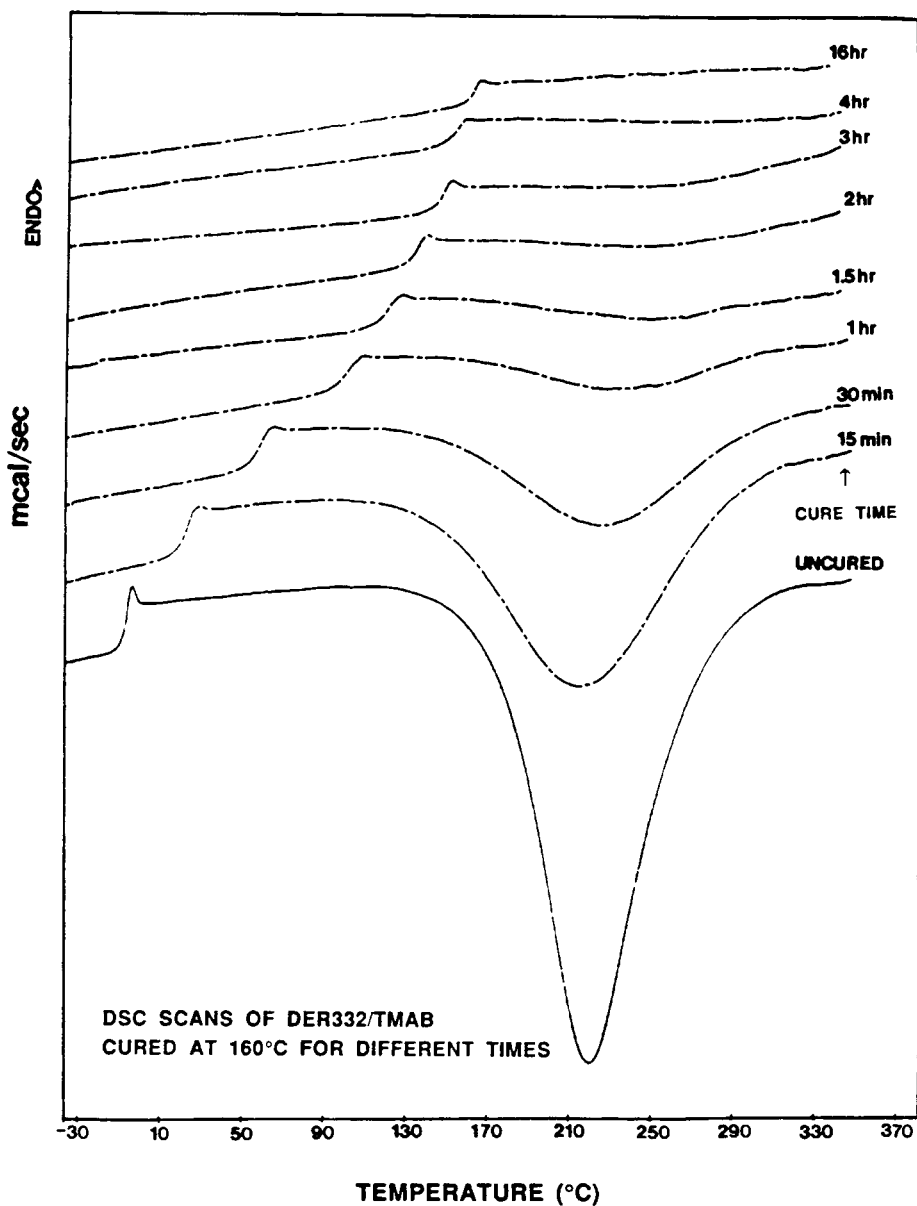
Fig. 5.   A series of DSC temperature scans of samples, cured isothermally at 160°C for different times, showing T_g increasing and the residual exotherm decreasing with increasing cure times.

temperatures below $T_{g\infty}$ are marked by arrows. The reaction rate after vitrification is diminished because of the effect of diffusion control causing the T_g data after vitrification to increase only slowly and appear to level off to lower limiting values for lower cure temperatures.

Treating the data as if the reaction is only kinetically controlled, neglecting, for the moment, the contribution of diffusion control, the reaction rate can be described mechanistically by the usual kinetic rate equation

RESIDUAL EXOTHERM VS. T_g FOR DER332/TMAB [DSC RESULTS]

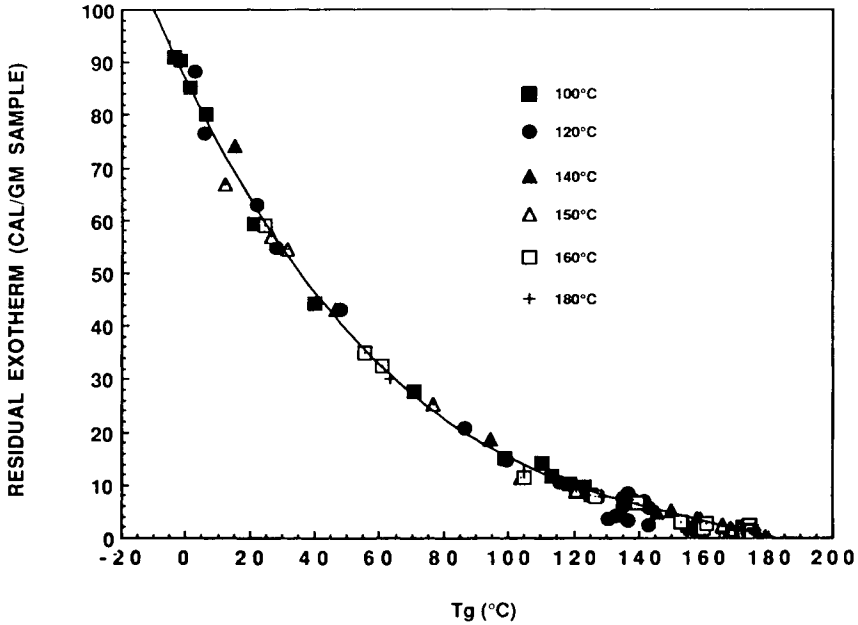y = 86.766 - 1.2612x + 6.8526e-3x^2 - 1.3973e-5x^3   R^2 = 0.998

Fig. 6.   Residual exotherms of partially cured materials cured at different temperatures plotted vs. the corresponding glass transition temperatures. The solid line represents a third-order polynomial fit of most of the data.

$$\frac{dx}{dt} = k(T) \times f(x) \tag{2}$$

where $k(T)$ is the reaction rate constant that is a function of temperature only, $f(x)$ is some function of conversion, and t is cure time.

Rearranging eq. (2), integrating at constant temperature, and taking the natural logarithm,

$$\ln\left(\int_0^x \frac{dx}{f(x)}\right) = \ln k(T) + \ln(t)$$

The left-hand side of the above equation is a function of conversion only and, equivalently therefore, a function of T_g only, i.e., $F(T_g)$. Therefore,

$$F(T_g) = \ln k(T) + \ln(t)$$

This equation describes the variation of T_g with cure time and temperature. Let T_g vary with time t_1 for cure temperature T_1, and with time t_2 for cure temperature T_2:
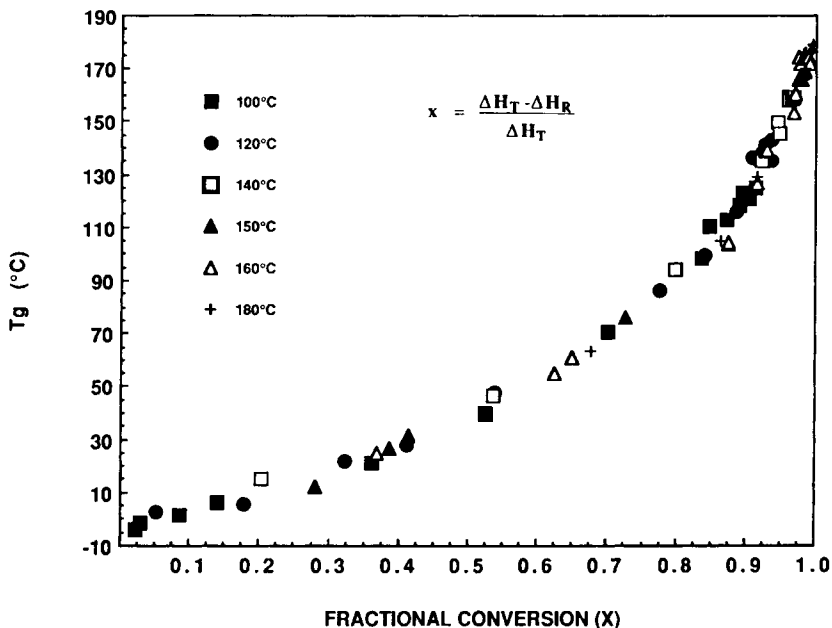
Tg vs. X FOR DER332/TMAB (1:1)

Fig. 7. The same data used in obtaining the polynomial fit in Figure 6 plotted as T_g vs. fractional conversion.

$$F(T_g) = \ln k(T_1) + \ln(t_1) = \ln k(T_2) + \ln(t_2) \qquad (3)$$

$$\ln(t_1) - \ln(t_2) = [\ln k(T_2) - \ln k(T_1)] \qquad (4)$$

For any two isothermal temperatures, $[\ln k(T_2) - \ln k(T_1)]$ is a constant. Therefore, for a kinetically controlled reaction, the variation of T_g with time at two different cure temperatures (T_1 and T_2) when plotted as functions of ln (time) will have the same functional form except that the curve for the cure temperature T_2 will be displaced from that of the temperature T_1 by a constant factor. It follows that if the reaction is solely kinetically controlled, all T_g vs. ln (time) curves at different cure temperatures should be superposable by simply shifting each curve along the ln (time) axis relative to a curve at an arbitrary reference temperature by a shift factor, $A(T) = [\ln(t_{ref}) - \ln(t_T)]$, for each temperature relative to the reference temperature.

The T_g vs. time data in Figure 8 are replotted vs. ln (time) in Figure 9. The resulting curves are shifted along the ln (time) axis in Figure 10 so that the beginning section ($T_g < 90°C$) of each curve coincides with that of the curve at $T_{cure} = 140°C$ in order to form a master curve at 140°C. The shift factors, $A(T)$, used in shifting the curves relative to $T_{cure} = 140°C$, are summarized in Table I.

It can be seen from Figure 10 that data prior to vitrification for all cure temperatures can be superimposed to form a convincing master curve. The vitrification points at different cure temperatures are designated on the master
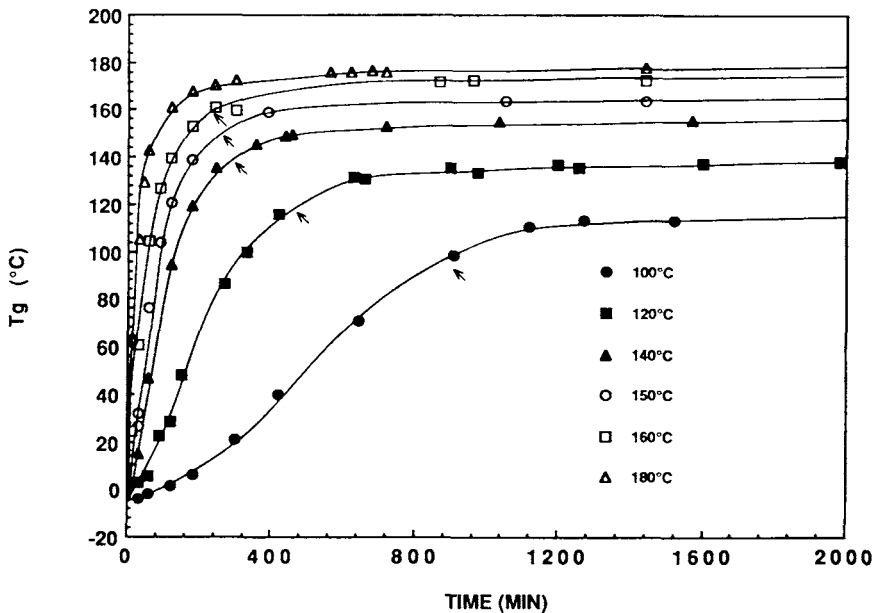
T_g vs. TIME FOR DER332/TMAB

Fig. 8. T_g vs. time at different cure temperatures. (Data were obtained for cure times up to 10,000 min at all cure temperatures; however, for clarity, only the results for cure times less than 2000 min are shown). Vitrification points for $T_{cure} < 180°C$ are marked by arrows. (Solid curves are hand-drawn.)

curve by arrows together with the corresponding cure temperatures. Data for cure temperatures less than 180°C branch off from the master curve shortly after the vitrification points because of the influence of diffusion control. The master curve represents the progression of T_g when the material is cured at 140°C if the reaction is only kinetically controlled. The fact that the isothermal vitrification points for all cure temperatures lie on the master curve indicates that prior to vitrification the reaction is primarily kinetically controlled; diffusion control of the reaction becomes influential only after vitrification.

Activation Energy

For a kinetically controlled reaction mechanism, the temperature dependence of the rate constant is generally given by an Arrhenius relationship:

$$k(T) = A_0 \exp(-E/RT) \tag{5}$$

where all parameters have usual Arrhenius significance and T is in units of absolute Kelvin.

The shift factors in Table I can be used to calculate the Arrhenius activation energy for the reaction, since eq. (4) provides the relationship between the time shift factors and the rate constants:
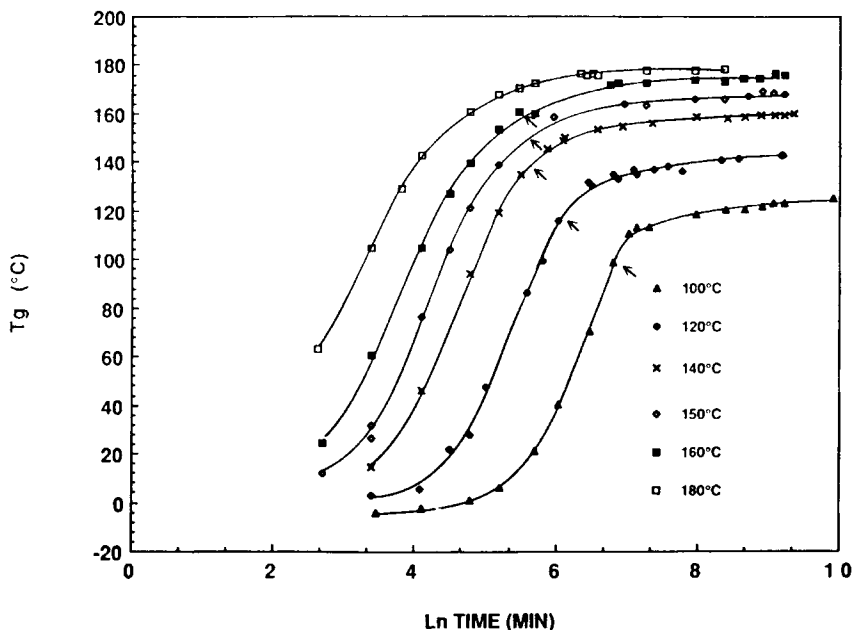
WISANRAKKIT AND GILLHAM

Tg vs. ln(TIME) FOR DER332/TMAB

Fig. 9. All T_g vs. time data at different cure temperatures of Figure 8 plotted in a ln(time) basis. Isothermal vitrification ($T_g = T_{cure}$) at each cure temperature is designated by an arrow. (Solid curves are hand-drawn.)

$$A(T) = \ln(t_{ref}) - \ln(t_T) = \ln k(T) - \ln k(T_{ref})$$

$$= -\frac{E}{RT} + \frac{E}{RT_{ref}} \tag{6}$$

When T_{ref} is fixed and all other data are shifted relative to the reference temperature (e.g., for the present case $T_{ref} = 140°C$), plotting the shift factor $[\ln(t_{ref}) - \ln(t_T)]$ against $1/T$ should yield a straight line with slope given by $-E/R$ and intercept equal to $E/(RT_{ref})$.

TABLE I
The ln(time) Shift Factor [$A(T)$] between T_{cure} and 140°C Used in Constructing the T_g vs. ln(time) Master Curve at 140°C (Fig. 10)

Cure temperatures (°C)	Shift factors [$A(T)$] = [$\ln(t_{140}) - \ln(t_T)$]
100	−1.986
120	−0.913
140	0.000
150	0.444
160	0.880
180	1.649

SUPERPOSITION OF KINETICALLY CONTROLLED T$_g$
AT DIFFERENT T$_{CURE}$

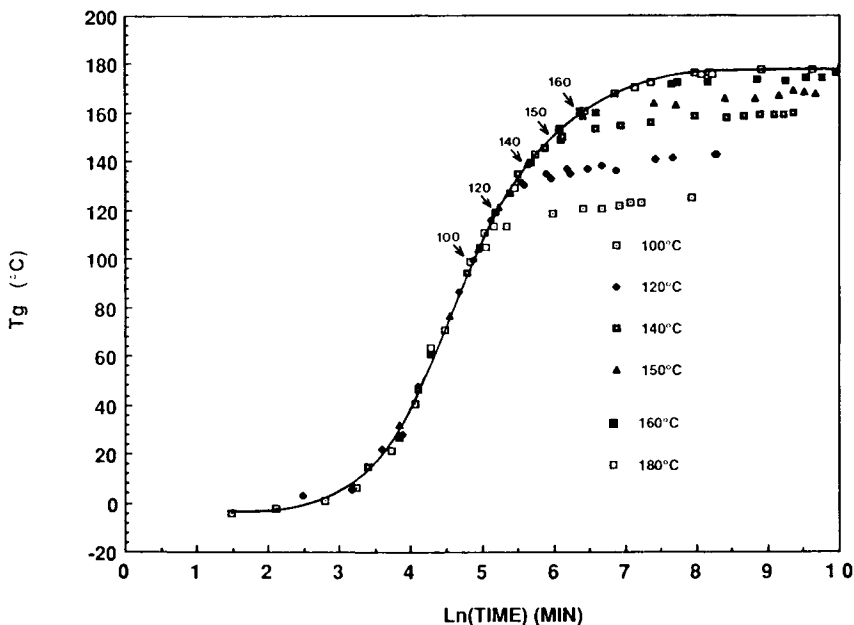Fig. 10. Superposition of the T_g vs. ln(time) data to form a master curve at 140°C by shifting each curve in Figure 9 by a constant factor $[A(T) = \ln(t_{140°C}) - \ln(t_T)]$ along the ln(time) axis so that its beginning section ($T_g < 90°C$) coincides with the curve for $T_{cure} = 140°C$. Isothermal vitrification points at different cure temperatures are marked by arrows. Note that vitrification points at all cure temperatures lie on the master curve.

The ln(time) shift factors in Table I are plotted vs. $1/T$ in Figure 11. The resulting plot is, in fact, a straight line, the slope of which yields an activation energy for the reaction of 15.23 kcal/mol (63.72 kJ/mol). These results also suggest for the present system that there is only one overall reaction mechanism with a single overall apparent activation energy.

Similar time-temperature superpositions have been used to calculate the activation energies for other amine-cured epoxy systems based on T_g vs. cure time[9,10] and conversion vs. cure time[11–13] at different cure temperatures. Those results also show the change from chemical-controlled to diffusion-controlled kinetics in the vicinity of isothermal vitrification.

Iso-T_g Contours and the Vitrification Curve in the Isothermal TTT Diagram

In recent work from this laboratory,[14,15] a simple methodology has been presented for the straightforward calculation of iso-T_g contours and the vitrification curve in the isothermal time-temperature-transformation (TTT) cure diagram from knowledge of the reaction activation energy and data points relating T_g-t_{cure}-T_{cure} over the entire range of T_g (e.g., T_g vs. time from $T_g = T_{g0}$ to $T_g = T_{g\infty}$ for one T_{cure}). The basic assumptions for this procedure are (i)
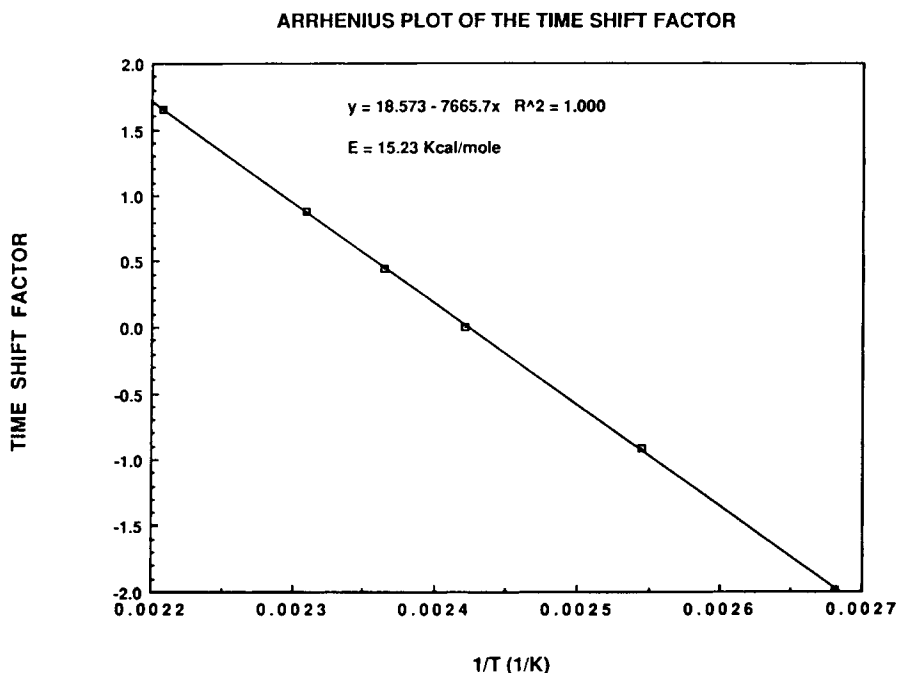
ARRHENIUS PLOT OF THE TIME SHIFT FACTOR

Fig. 11.   Arrhenius plot of the shift factors, $A(T)$, used in constructing the master curve in Figure 10 vs. $1/T(K)$. The activation energy for the reaction is determined from the slope of the straight line.

the reaction prior to vitrification is kinetically controlled, and (ii) there is a unique one-to-one relationship between T_g and chemical conversion.

   The relationship between the times to reach a fixed T_g at different cure temperatures for a kinetically controlled reaction is given by eq. (6), recast as follows:

$$-\frac{E}{RT_1} + \ln(t_{T_g^*,1}) = -\frac{E}{RT_2} + \ln(t_{T_g^*,2}) \qquad (7)$$

where $t_{T_g^*,1}$ is the time needed to reach a given glass transition temperature, T_g^*, at cure temperature T_1 and $t_{T_g^*,2}$ is the time needed to reach the same T_g at cure temperature T_2. Thus, if a time to reach a particular T_g at one cure temperature (i.e., $t_{T_g^*,1}$ at T_1) is known, then the times to reach the same T_g at different temperatures (i.e., $t_{T_g^*,2}$ at any T_2) can be calculated from eq. (7) provided that the reaction activation energy is available. The times to reach a fixed T_g^* at different cure temperatures when plotted as T_{cure} vs. cure time constitute an iso-$T_g = T_g^*$ line in the TTT cure diagram. To calculate all possible iso-T_g contours, data points relating T_g-t_{cure}-T_{cure} under kinetically controlled conditions over the entire range of T_g are required.

   When T_2 is equal in value to the glass transition temperature, T_g^*, the time $t_{T_g^*,2}$ calculated from eq. (7) is the time to reach isothermal vitrification when the material is cured at the T_g^* value. Vitrification points for all possible values of T_g^* (i.e., from $T_g^* = T_{g0}$ to $T_g^* = T_{g\infty}$), when plotted in the form of T_{cure} vs. cure time, constitute the vitrification curve in the TTT diagram.

For the present system, the reaction is found to be kinetically controlled up to the vitrification points, and a one-to-one relationship between T_g and conversion is evident from the experimental results in Figure 7, for the entire range of T_{cure} investigated (100–180°C). Therefore, it appears that eq (7) can be applied directly to the calculation of the vitrification curve and the iso-T_g contours.

Figure 12 shows the master curve of the shifted T_g vs. ln(cure time) data of Figure 10 excluding the branched data at cure temperatures less than 180°C due to the effect of diffusion control. This curve represents the variation of T_g with cure time at 140°C when the reaction is kinetically controlled (i.e., the reaction proceeds at 140°C from an uncured state to a fully cured state without the interference of vitrification or diffusion control). Each point on the master curve provides a necessary datum point [i.e., a time ($t_{T_g^*,1}$) to reach a particular T_g^*, at $T_1 = 140$°C], which can be used in eq. (7), together with the activation energy for the reaction determined in the previous section, for the calculation of an iso-$T_g = T_g^*$ contour. Since the master curve covers the entire range of T_g, any desired iso-T_g contour, as well as the vitrification curve, can be calculated.

Figure 13 shows the calculated vitrification curve and different iso-T_g contours (for $T_g = -4, 0, 4, 10, 20, \ldots, 160, 170, 175,$ and 177°C) in the form of an isothermal TTT diagram. The calculated vitrification curve is S-shaped, which is also observed by direct experiments.[1-4] The maximum time to vitrification

Tg VS Ln(t) MASTER CURVE AT 140°C

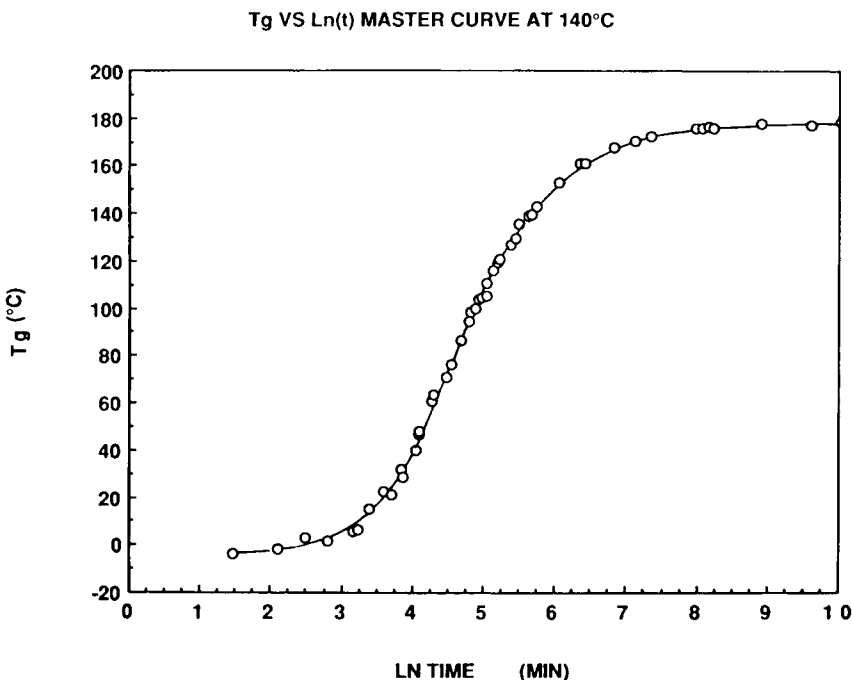Fig. 12. The kinetically controlled T_g vs. ln(time) curve at 140°C derived from the time-shift plot in Figure 10, excluding data at cure temperatures lower than 180°C that branch off from the master curve due to the effect of diffusion control after vitrification. Shifted experimental data (symbols); hand-fitted curve (solid curve).
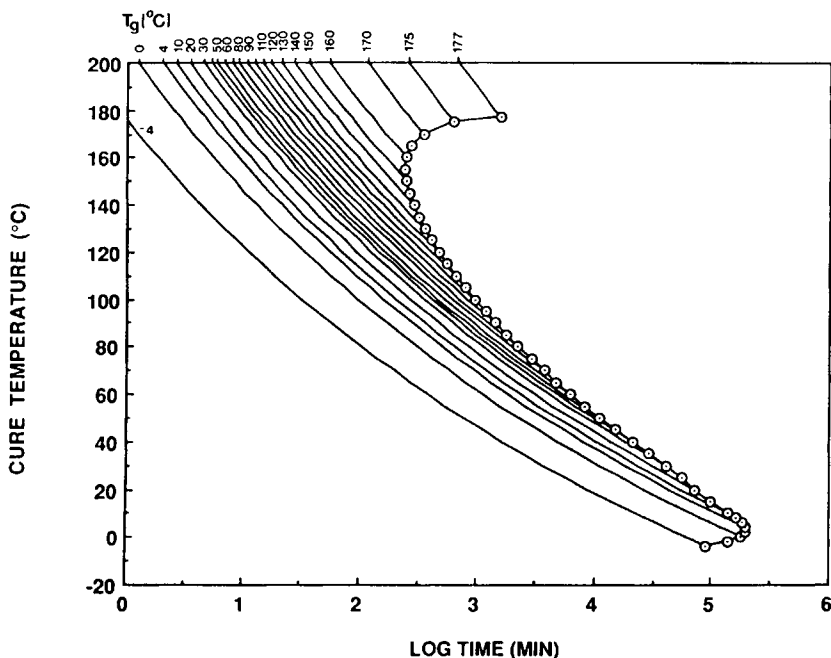
WISANRAKKIT AND GILLHAM

Fig. 13. Calculated isothermal TTT diagram showing iso-T_g contours and the vitrification curve. Calculations for the iso-T_g contours were performed using eq. (7), the T_g vs. ln(time) data of the kinetically controlled master curve at 140°C in Figure 12, and the activation energy obtained from the shift factors used to obtain the kinetically controlled master curve at 140°C.
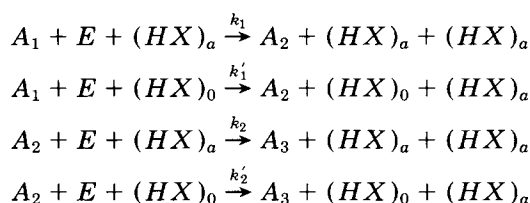
at low temperature can be considered to be due to the opposing influences of the temperature dependencies of the viscosity and the reaction rate constant.[1] The minimum time to vitrification at high temperature is a consequence of the opposing influences of the increasing reaction rate constant and the decreasing concentration of reactants at vitrification with increase of temperature.[4] For highly reactive systems, the vitrification curve can be conveniently obtained directly by experimental techniques such as torsional braid analysis (TBA).[1] However, for slow to moderately reactive systems (such as the present epoxy/amine system), it would be quite impractical to construct the complete vitrification curve directly, especially in the low-temperature range (near T_{g0}) since the material would take considerable time to vitrify (e.g., the calculated vitrification time at 0°C for the current system is approximately 120 days). Therefore, from a practical point of view, the above calculation procedure provides a convenient means for calculating the entire vitrification curve from limited short-time data at high cure temperatures.

   The iso-T_g contours appear as a series of parallel lines in the TTT diagram. It is interesting to note that the contours are farther apart at the beginning of cure (-4°C $< T_g < 30$°C), become closer together in the middle of cure (30°C $< T_g < 130$°C), and spread apart again in the later stages of cure (130 $< T_g$ < 178°C $= T_{g\infty}$). The characteristics in the initial stages is a combination effect of the autocatalyzed reaction (for which the reaction rate is maximum at $t > 0$)

and the presentation in the log time scale (which spreads out the short-time data and contracts together the long-time data). The feature in the later stages of cure is mainly due to low reaction rate toward high conversion.

Autocatalyzed Reaction Kinetics

The curing of epoxy with primary amine involves two principal reactions: the reaction between primary amine hydrogen and epoxy to form secondary amine, and the reaction between secondary amine hydrogen and epoxy to form tertiary amine (Fig. 2). Both reactions are found to be catalyzed by the hydroxyl groups formed during the reaction.[16] Horie et al.[17] have derived the following scheme to describe the overall kinetics of the epoxide reaction with primary amine, taking into account the autocatalytic action of the hydroxyl groups generated during the reaction and assuming that some catalyst or impurity is initially present in the system:

$$A_1 + E + (HX)_a \xrightarrow{k_1} A_2 + (HX)_a + (HX)_a$$
$$A_1 + E + (HX)_0 \xrightarrow{k_1'} A_2 + (HX)_0 + (HX)_a$$
$$A_2 + E + (HX)_a \xrightarrow{k_2} A_3 + (HX)_a + (HX)_a$$
$$A_2 + E + (HX)_0 \xrightarrow{k_2'} A_3 + (HX)_0 + (HX)_a$$

where A_1, A_2, and A_3 are primary, secondary, and tertiary amine, respectively; E is the epoxy group; $(HX)_a$ is the pendant hydroxyl groups on the backbone of the reaction products; and $(HX)_0$ is the initial catalyst or impurities. The rate constants for the individual reactions are defined in the scheme. $(HX)_a$ and $(HX)_0$ are assumed to act as catalysts with no net consumption by side reactions.

Assuming equal reactivity of all amino hydrogens, the reaction rate for an initial stoichiometric mixture of epoxy and amine can be expressed on a fractional conversion basis (x) as (see Appendix A for more details)

$$\frac{dx}{dt} = k(1 - x)^2(x + B) \tag{8}$$

where $k = k_1 e_0^2/2$, $B = k_1' c_0/k_1 e_0$, and e_0 and c_0 are the initial concentrations of epoxide groups and $(HX)_0$, respectively.

This rate expression has the general form of eq. (2), in which $f(x) = (x + B)(1 - x)^2$ is assumed to be independent of cure temperature. The constant B in $f(x)$ is at most only a weak function of temperature since the rate constants k_1 and k_1' are expected to have a similar temperature dependence, and their ratio will be approximately constant for all temperatures. Equation (8) is used to analyze the reaction kinetics of the present system by rearranging in the following form:

$$\frac{dx/dt}{(1 - x)^2} = kx + kB \tag{9}$$

The data of the T_g master curve at 140°C in Figure 12 are converted into a fractional conversion basis through the use of the fitting polynomial of Figure 6. The results are shown in Figure 14 and are used for the kinetic analysis according to eq. (9). The best local fit solid line drawn through the data points is used for the evaluation of the reaction rate, dx/dt, corresponding to the conversion x. Figure 15 presents a plot of $(dx/dt)/(1 - x)^2$ vs. fractional conversion, x. The resulting plot can be correlated with a straight line depicting eq. (9) up to 85% conversion. The slope of the straight line, related to the rate constant k_1 at 140°C with a multiplicative constant $e_0^2/2$, is equal to $6.6793E - 2$. The y-intercept together with the knowledge of k gives a value of constant B equal to $5.548E - 2$. The nonzero value of B indicates the presence of initial trace catalyst accelerating the reaction in the system. This could be either a small amount of impurities of hydroxyl groups initially in the diepoxide monomer and those due to an initial extent of reaction occurring during mixing of the reactants.

The parameters (k and B) determined from the plot are substituted back in eq. (8), and the resulting first-order ordinary differential equation is integrated numerically to obtain the fractional conversion at 140°C as a function of time. The results of the integration are presented in Figure 16 (solid line) together with the experimental data from the master curve (circles). It is apparent that the chemical kinetics for the reaction of this epoxy/amine system can be sat-

KINETICALLY CONTROLLED X VS. TIME AT 140°C

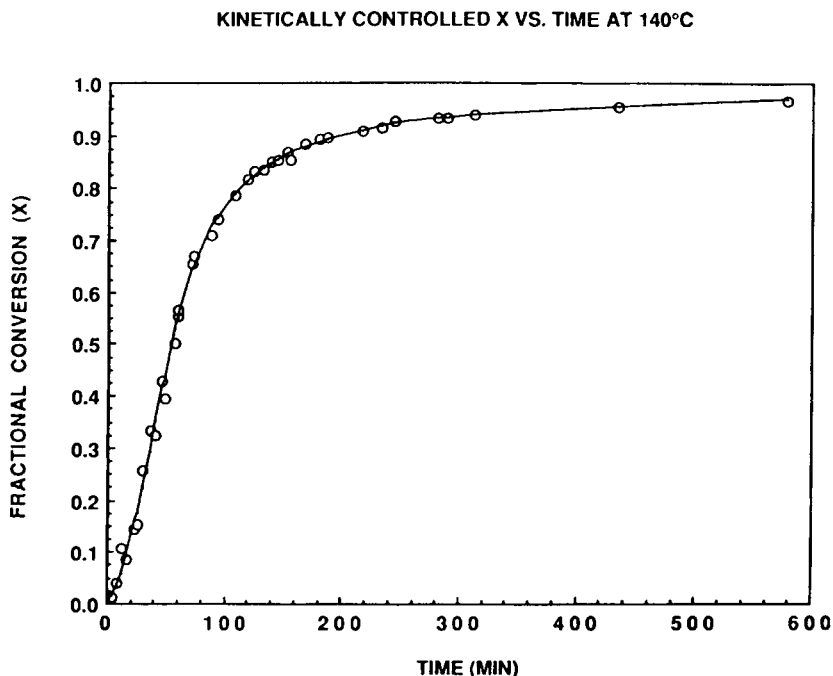Fig. 14.   The kinetically controlled fractional conversion vs. time at 140°C derived from the T_g vs. ln(time) data in Figure 10 by converting the T_g data into fractional conversion data using the relationship established in Figure 6. Data points from Figure 10 (circles); best local fit (solid curve).

DETERMINATION OF AUTOCATALYTIC KINETIC PARAMETERS
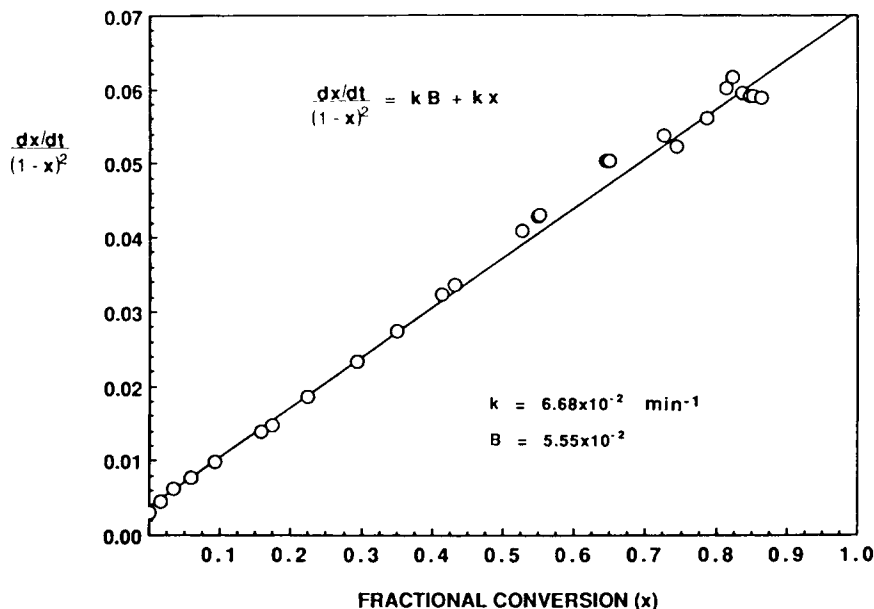
y = 3.7056e-3 + 6.6793e-2x   R^2 = 0.997

Fig. 15. The data in Figure 14 analyzed according to autocatalyzed reaction kinetics. The parameters for the kinetic rate expression are determined from the slope and intercept of the linear least-square fit of the data (solid line).

isfactorily represented by the simple autocatalyzed kinetics throughout the entire conversion range.

It might be inferred from the unique one-to-one relationship between T_g and conversion, which is independent of the cure temperature, that the ratio of the rate constant for the reaction between the primary amine group and epoxy to that between the secondary amine group and epoxy, k_1/k_2, is a constant that is independent of temperature. The relationship could also imply that the activation energies for both reactions are the same. Furthermore, the agreement between the experimental data and the results of the calculations from the assumed kinetics suggests that all amino hydrogens react with equal reactivity (i.e., $k_2/k_1 = 0.5$) or only with a weak negative substitution effect. This assumption has also been found to be valid for other aromatic amine-cured epoxy systems by several investigators.[18-20] The sensitivity of the assumed kinetic calculations to different reactivity ratios is presented in Appendix B. The analysis shows that the value of k_2/k_1 is between 0.4 and 0.5.

The autocatalytic reaction model has been used by other investigators to describe the chemical kinetics of a variety of aromatic amine-cured epoxy systems[21-25] and has been found to be applicable over a wide conversion range for curing before vitrification. In those investigations, the long-time results at low-temperature curing after vitrification typically deviated from the kinetic model predictions. Obviously, these deviations are expected as the reactions become diffusion limited after the materials vitrify. However, very few studies have attempted to incorporate the effects of diffusion control into the reaction

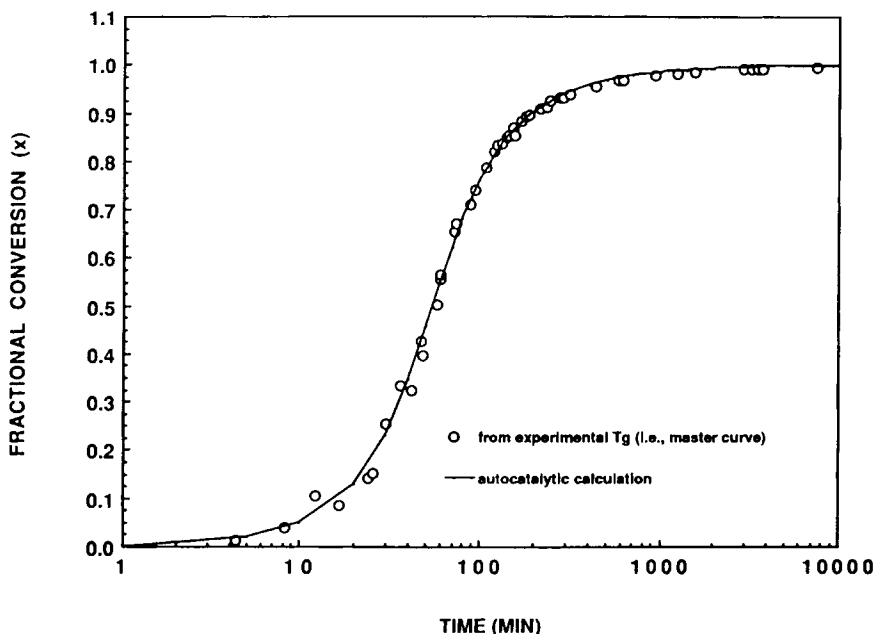**KINETICALLY CONTROLLED CONVERSION VS. TIME AT 140°C (MASTER CURVE)**

Fig. 16. The numerical integration results of the autocatalytic rate expression, eq. (8) at 140°C (using the parameters determined in Fig. 15), compared with the experimental results. Autocatalytic calculation (solid curve); from experimental T_g data (symbols).

kinetic model. Havlicek and Dusek[26] have presented a theoretical approach to take into account the influence of diffusion control on the reaction kinetics, particularly in the glass transition region of amine-cured epoxy systems. In the following section, this approach with some modifications is used in order to account for the deviation beyond vitrification of the conversion (and T_g) data from the kinetically controlled calculations.

Diffusion-Controlled Kinetics

In the previous section, the chemical kinetics for the reaction of the present amine-cured epoxy system has been shown to be autocatalyzed and, in the absence of diffusion control, can be adequately represented by an Arrhenius-type overall rate constant with a single overall activation energy. In actuality, however, diffusion of chain segments can become a dominating factor especially when the T_g of the material rises beyond the cure temperature (i.e., after vitrification). The influence of diffusion control can be clearly inferred in Figure 10 from the branching off of the T_g data from the kinetically controlled master curve shortly after vitrification for all $T_{cure} < 180°C$ data.

The time scale for the overall reaction is a sum of the time for diffusion of reactants and the time for chemical reaction. When a reaction is diffusion-controlled, the diffusion of chemical reactants becomes a limiting step. The effect of diffusion control can be incorporated into the kinetics of the reaction

by modifying the rate constant using the Rabinowitch model[27] as suggested by Havlicek and Dusek[26] as follows:

$$\frac{1}{k_a(x, T)} = \frac{1}{k_T(T)} + \frac{1}{k_d(x, T)} \tag{10}$$

where k_a is the overall rate constant, k_T is the scaled kinetic (Arrhenius) rate constant ($k_T = k_1 e_0^2/2$, which assumes equal reactivity of primary and secondary amino hydrogens), and k_d is the diffusion rate constant. All rate constants in eq. (10) have units of (min)$^{-1}$. This equation shows that the overall rate constant is governed at one extreme by the Arrhenius rate constant (when $k_d \gg k_T$), which is the case prior to vitrification, and at the other extreme by the diffusion rate constant (when $k_T \gg k_d$), which is the case well after vitrification.

According to the generally accepted view of relaxation processes controlled by diffusion of molecular chain segments in the glass transition region of amorphous polymers, the molecular relaxation time can be described by the well-known Williams–Landel–Ferry (WLF) equation,[28] which is modified in the following form[29,30] to permit application both above and below T_g:

$$\log(a_T) \equiv \log \frac{\tau(T)}{\tau(T_0)} = -\frac{C_1(T - T_0)}{C_2 + |T - T_0|}$$

where T is the temperature of the experiment, T_0 is an arbitrary reference temperature, C_1 and C_2 are constants, $\tau(T)$ and $\tau(T_0)$ are the polymer segmental relaxation times at the temperatures T and T_0, respectively, and a_T is the time-temperature superposition factor. When T_0 is chosen as the dilatometric glass transition temperature, the value of C_1 and C_2 are generally found to be nearly constant equal to 17.44 and 51.6°C, respectively, for many amorphous polymers.[28] The difference between the usual WLF equation and the above modified form is the inclusion of the absolute value $|T - T_0|$ in the denominator that allows application of this relationship below T_g.[29] (The usual form of the WLF equation applies only above T_g under equilibrium conditions. The present analysis neglects this and also neglects consideration of the effects of spontaneous densification [i.e., physical aging] below T_g which also affects the mobility of reactive sites.)

The rate constant for chemical reaction governed by the diffusion of chain segments, k_d, can be expected to be proportional to the diffusion constant of the reactants, or equivalently, to be inversely proportional to the relaxation time of the polymer segments.[31] This suggests that the temperature dependence of k_d would be in the following form:

$$\log \frac{k_d(T)}{k_d(T_g)} = \frac{C_1(T - T_g)}{C_2 + |T - T_g|}$$

or in a natural logarithmic form,

$$\ln[k_d(T)] = \ln[k_d(T_g)] + \frac{2.303 C_1(T - T_g)}{C_2 + |T - T_g|}$$

Assuming $k_d(T_g)$ is a constant denoted as k_{d0}, and letting $\alpha = 2.303C_1$, the above equation becomes

$$\ln(k_d) = \ln(k_{d0}) + \frac{\alpha(T - T_g)}{51.6 + |T - T_g|} \qquad (11)$$

In this work, the value of C_2 is taken as 51.6°C, whereas the values of k_{d0} and α will be determined from a fit of the experimental data after vitrification at 140°C.

Data after vitrification of T_g vs. time at $T_{cure} = 140$°C are used for the determination of k_{d0} and α at 140°C. The procedure is as follows: (i) The actual experimental overall rate constants, k_a, for the later stages of the reaction at 140°C are evaluated from the T_g vs. time data, from which the diffusion rate constants at 140°C can be determined using eq. (10); and (ii) plotting $\ln(k_d)$ vs. $(T - T_g)/[51.6 + |T - T_g|]$ should yield a straight line, the slope and y-intercept of which can be used for calculating α and k_{d0}, respectively, at 140°C.

(i) Evaluation of k_d

Figure 17 shows the experimental T_g vs. ln(time) data at 140°C used in the calculation. It is noticed that the T_g vs. ln(time) data after vitrification for $t > 1000$ min can be approximated by a straight line:
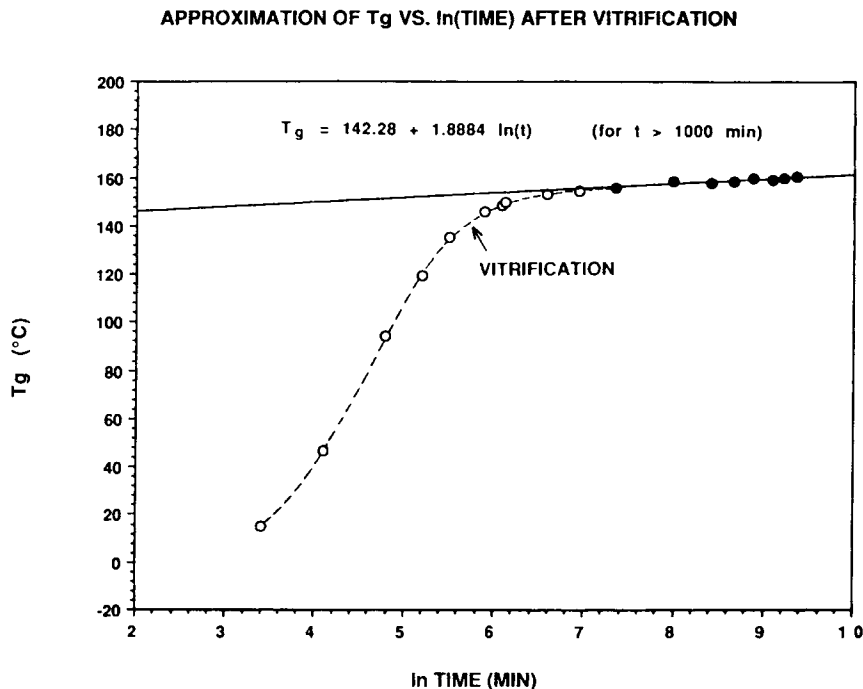
APPROXIMATION OF Tg VS. ln(TIME) AFTER VITRIFICATION

Fig. 17. Experimental T_g vs. ln(time) data (symbols) at 140°C showing the approximation by a straight line of the long time data (solid circles) after isothermal vitrification (marked by an arrow).

$$T_g = 142.28 + 1.8884 \ln(t) \qquad (\text{for } t \gg t_{vit}) \qquad (12)$$

The rate of conversion in this range can be calculated from this relation by

$$\frac{dx}{dt} = \frac{dx}{dT_g} \cdot \frac{dT_g}{dt} = \frac{dx}{dT_g} \cdot \frac{1.8884}{t} \qquad (13)$$

The term, dx/dT_g, is directly calculated from the fitting polynomial between x and T_g. Thus, for any given time > 1000 min, the corresponding T_g, x, and dx/dt can be determined from eq. (12), the fitting polynomial between T_g and x, and eq. (13), respectively. The values of x and dx/dt are then used to compute the actual overall rate constant, k_a, from the autocatalytic rate expression, eq. (8):

$$k_a = \frac{dx/dt}{(1 - x)^2 (x + B)}$$

The kinetically controlled rate constant, k_T, is the same Arrhenius rate constant determined earlier. The diffusion rate constant follows directly from eq. (10):

$$\frac{1}{k_a} = \frac{1}{k_T} + \frac{1}{k_d} \rightarrow k_d = \frac{k_a k_T}{k_T - k_a}$$

The values of T_g and k_d are evaluated at 140°C for time > 1000 min (for which eq. (12) is valid) at every 100 min interval up to $t = 10,000$ min.[7]

(ii) Evaluation of k_{d0} and α

The natural logarithm of the computed k_d at 140°C is plotted against $(T - T_g)/[51.6 + |T - T_g|]$ in Figure 18. The resulting plot is, in fact, a straight line as suggested by eq. (11). The slope and y-intercept give the values of α and $\ln(k_{d0})$ equal to 42.61 and 3.4223, respectively. Therefore, the expression for k_d at 140°C becomes

$$k_d = 30.64 \exp\left[\frac{42.61(T - T_g)}{51.6 + |T + T_g|} \right] \qquad (14)$$

The value of α determined from the fit of the data is actually very close to the familiar value of the general WLF equation (for which when $T_0 = T_g$, $C_1 = 17.44$, and since $\alpha = 2.303 C_1$, $\alpha = 2.303 \times 17.44 = 40.2$). This agreement provides further assurance in using the assumed form of k_d.

The diffusion rate constant, k_d, given by eq. (14) and the kinetic Arrhenius rate constant, k_T, are substituted in eq. (10) to evaluate the overall rate constant k_a at 140°C. As a consequence, k_a become a function of both the T_g, which varies with cure time, and the cure temperature. The expression for k_a is then substituted in the autocatalytic rate expression, eq. (8). The resulting differential equation has the form

WISANRAKKIT AND GILLHAM

DIFFUSION PARAMETERS DETERMINATION
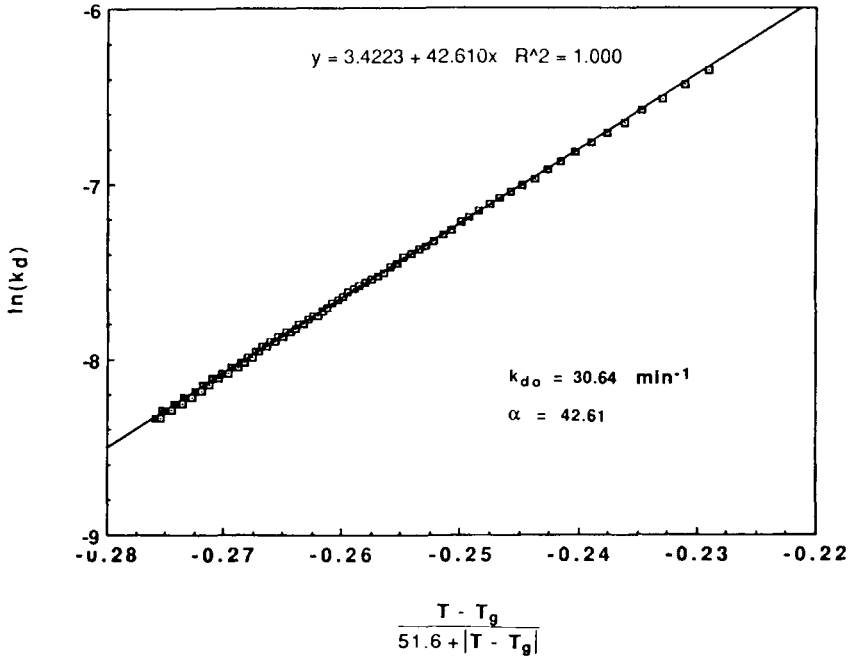**FROM DATA AFTER VITRIFICATION AT 140°C**

Fig. 18. Determination of the diffusion-controlled kinetic parameters in eq. (11) at 140°C. The calculated values for $(T - T_g)$ and the corresponding k_d values (symbols) were evaluated from the long time T_g vs. ln(time) straight line plot at 140°C in Figure 17 at 100 min intervals from $1000 < t < 10,000$ min. Resulting data are fitted with a straight line.

$$\frac{dx}{dt} = f(x, T_g(x), T) \qquad \text{with } x(t = 0) = 0$$

which can be integrated numerically at each temperature to obtain the conversion as a function of time, assuming that the WLF parameters are independent of temperature. The numerical integration was performed for different cure temperatures (100, 120, 140, 150, 160, and 180°C). The results of the calculation are shown in Figure 19 together with the conversion data determined from the experimental T_g values at each cure temperature. The corresponding calculated results for T_g vs. time and the experimental T_g data are shown in Figure 20. Agreement between calculation results and the experimental data is good. (If valid, it follows that the segmental relaxation times in the glass transition region are independent of the glass transition temperature [i.e., conversion].)

The overall reaction rate constant given by eq. (10) allows for either chemical or diffusion control dominating the reaction kinetics depending on the interval between T_g and the cure temperature. For a given isothermal cure temperature, the Arrhenius rate constant, k_T, does not change with time. The value of k_d, on the other hand, depends on the difference between T_g and T_{cure}. In the earlier

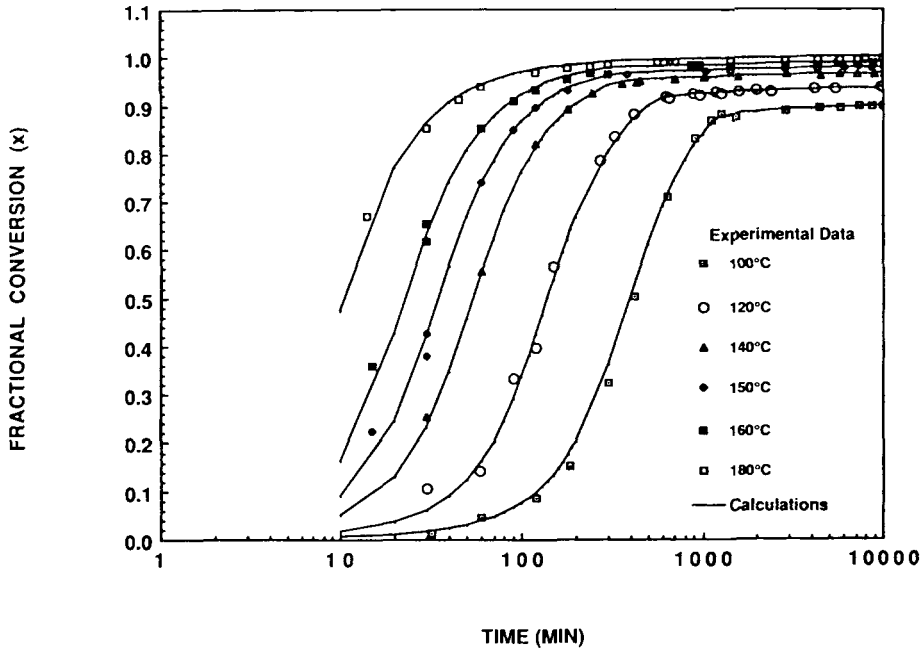FRACTIONAL CONVERSION VS. TIME: DIFFUSION CONTROLLED KINETICS

TIME (MIN)

Fig. 19. Results of the numerical integration for fractional conversion vs. log time at different temperatures of the kinetic rate expression in which the effect of diffusion has been included by modifying the overall reaction rate constant according to eq. (10) (solid line), compared with converted experimental data of Figure 9 (symbols).

stages of the reaction when $T_g \ll T_{\text{cure}}$, k_d is much greater than k_T since the sign of the term in the exponent of eq. (14) is positive (e.g., at $T_{\text{cure}} = 140°C$ and $T_g = 10°C$, $k_d = 5.4E + 14 \gg k_T = 6.7E - 2$). As a result, $1/k_T \gg 1/k_d$, and from eq. (10), $k_a \approx k_T$. Consequently, the reaction in the early stages is primarily kinetically controlled. As the reaction proceeds, T_g rises and approaches T_{cure}. The value of k_d becomes smaller, since $(T - T_g)$ becomes less, whereas the value of k_T remains constant at the given cure temperature. After vitrification (when $T_g > T_{\text{cure}}$), k_d becomes much smaller than k_T since the sign of the term in the exponent of eq. (14) is negative (e.g., at $T_{\text{cure}} = 140°C$ and $T_g = 160°C$, $k_d = 2.1E - 4 \ll k_T = 6.7E - 2$). Therefore, $1/k_T \ll 1/k_d$, and $k_a \approx k_d$, resulting in the reaction being dominated by diffusion-controlled kinetics.

Figure 21 shows the calculation for x vs. t at 140°C using the overall rate constant, eq. (10) compared with the calculation using only an Arrhenius rate constant (same as the calculated curve in Fig. 16), together with the experimental data points at 140°C. The corresponding calculations on a T_g basis are shown in Figure 22. Both calculations give the same result in the initial stages of the reaction (where chemical-controlled kinetics dominates). After vitrification (marked by an arrow), however, diffusion control retards the reaction substantially and only the model calculation incorporating the effect of diffusion satisfactorily accounts for the material behavior.
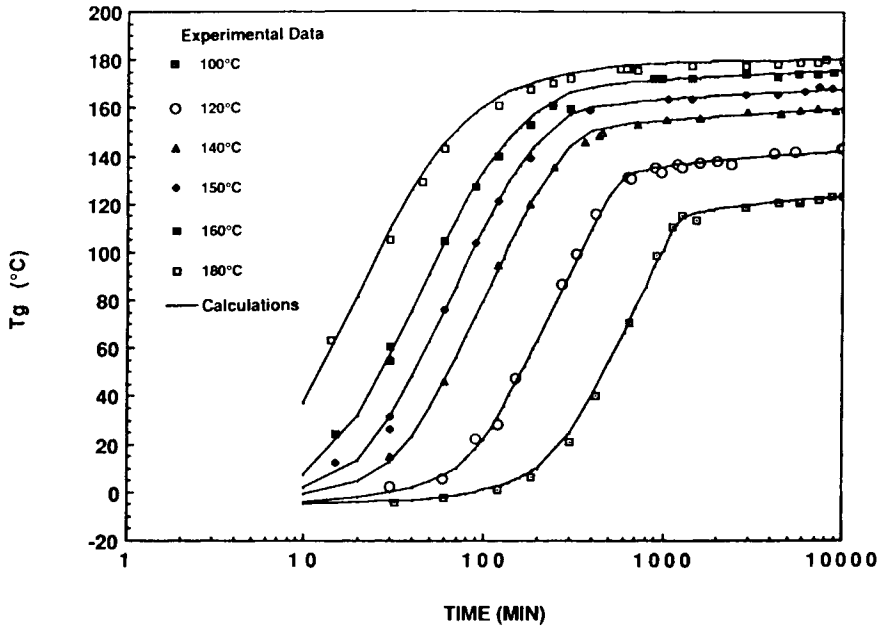
Tg VS. TIME: DIFFUSION CONTROLLED KINETICS

Fig. 20. Results of the numerical integration for T_g vs. log time at different temperatures of the kinetic rate expression in which the effect of diffusion has been included by modifying the overall reaction rate constant according to eq. (10) (solid line), compared with the experimental data of Figure 9 (symbols).

Variation of T_g with Conversion: Model Calculation

The analyses and calculations in the previous sections have been performed using the experimental T_g vs. time data: The reaction activation energy was found, the iso-T_g contours and the vitrification curve in the TTT diagram were calculated, and the reaction kinetics and diffusion-controlled rate expression were determined. Although most of the calculations and discussions can be made more directly on a reaction conversion basis, T_g is used since it is sensitive to small changes in conversion (particularly at high conversion) and can be determined more accurately than can the actual conversion data. As has already been demonstrated, these features of T_g are also especially useful in the analysis of the diffusion-controlled kinetics for which the rate of change in chemical conversion is small. However, the advantages of using T_g rely on the assumption that there is a unique one-to-one relationship between T_g and conversion. Furthermore, assuming equal reactivity for the amino/epoxy reactions, a kinetic model has been obtained that appears to describe satisfactorily the rate of cure before and after vitrification in terms of changing T_g as well as of conversion. In view of the preceding developments, it is of interest to establish a more fundamental molecular basis to support this hypothesis of the one-to-one relationship between T_g and chemical conversion.

It is apparent from Figure 7 that T_g relates to conversion in a nonlinear fashion with T_g rising more sharply with small increases in conversion at high

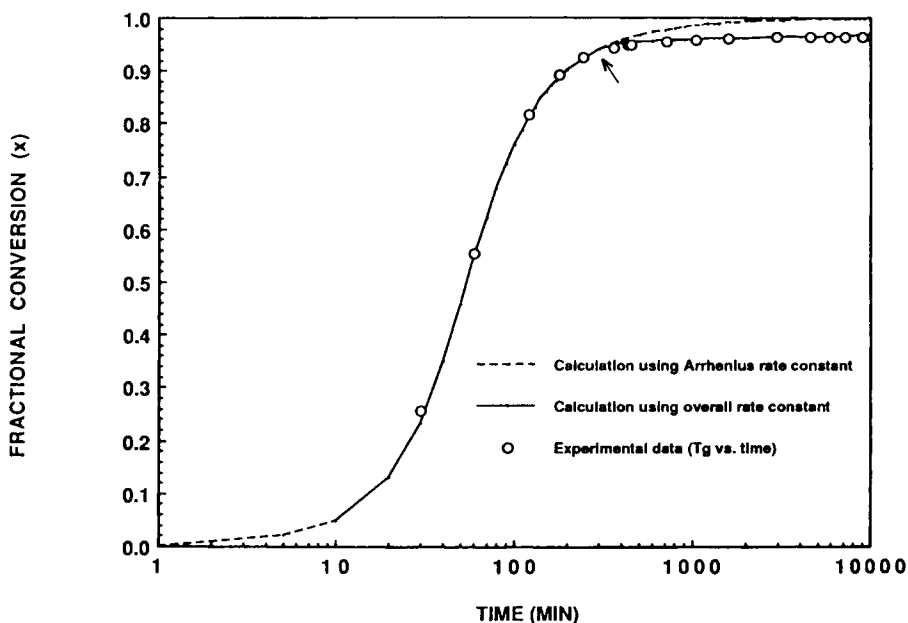**X VS. TIME AT 140°C FOR DER332/TMAB WITH DIFFUSION CONTROLLED KINETICS**

Fig. 21. Calculations at 140°C for fractional conversion vs. log time using the overall rate constant (solid line); using only the Arrhenius rate constant (dashed line). Experimental data at 140°C from Figure 9 (circles). Isothermal vitrification marked by an arrow.

conversions. This characteristic is considered to arise from the dependence of T_g on the functionality of the crosslinking units;[10,32] higher-functional crosslinking units (i.e., for this system, tetrafunctional amines with all four arms leading out to an infinite network) are more effective in raising T_g than are lower-functional crosslinking units (i.e., amines with only three of the four arms leading to an infinite network). The concentration of the higher functional crosslinking units increases at high conversion at the expense of the lower functional crosslinking units,[33,34] resulting in T_g rising more sharply at high conversion.

Previous work in this laboratory has attempted to theoretically model the relationship between T_g and conversion.[35] The model provides a clear fundamental basis for the variation of T_g with increasing conversion, but fails to give satisfactory correlation between calculation and experimental results. The following theoretical model is a modification of the previous attempt by taking into account the effectiveness of various functional crosslinking units in raising the T_g of the material.

For the curing of many thermosets, low molecular weight liquids are transformed into an infinite network of amorphous solid (glassy or elastomeric) polymer. Initially, all molecules are finite (sol). As the extent of reaction increases, T_g increases because of an increase in the molecular weight. After the chemical gel point (incipient formation of an infinite molecular weight molecule), the system is composed of both sol and gel (infinite molecule) fractions.
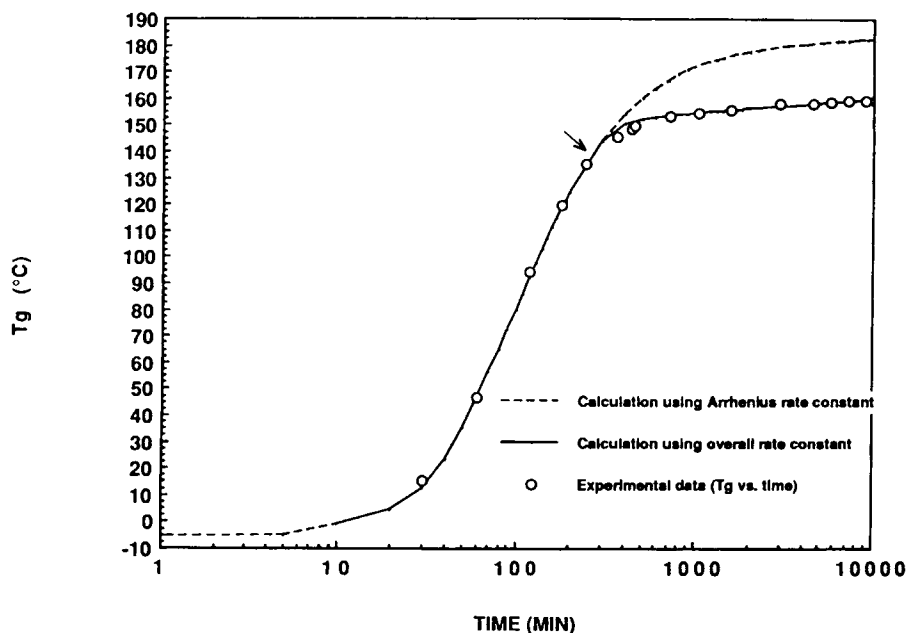
Tg VS. TIME AT 140°C WITH DIFFUSION CONTROLLED KINETICS

Fig. 22.   Calculations at 140°C for T_g vs. log time using the overall rate constant (solid line); using only the Arrhenius rate constant (dashed line). Experimental data at 140°C from Figures 9 (circles). Isothermal vitrification marked by an arrow.

Both species contribute to the overall increase of the T_g of the material. The T_g of the sol fraction is considered to be a function of its number average molecular weight, whereas that of the gel fraction depends on the crosslink concentration and depends more strongly on the higher functional crosslinking units than on the lower functional ones.

In the following model, the usual simplifying assumptions are made: All functional groups of the same type are equally reactive; all groups react independently; and only intermolecular reactions occur.

T_g before Gelation

According to Flory's theory of gelation,[33] a crosslinking system will gel molecularly when its fractional conversion, x, reaches a constant critical value given by

$$x_{gel} = \frac{1}{[r + r\rho(f - 2)]^{1/2}} \tag{15}$$

where f is the functionality of the crosslinking groups (i.e., 4 for the tetra-functional aromatic amine), r is the molar ratio of reacting functional groups (i.e., the molar ratio of epoxy group to amino hydrogen; for a stoichiometric mixture of reactants, $r = 1$), and ρ is the fraction of reactive sites of one type

in the branching units with that type (for the present system with only tetra-functional amines, $\rho = 1$).

For the stoichiometric curing of diepoxide with tetrafunctional amine in the present system ($f = 4$, $\rho = 1$, and $r = 1$), the theoretical fractional conversion at the gel point is 0.58. This critical gel point is used to divide the conversion range into two regions; one with only sol ($0 \leq x < 0.58$) and the other with a mixture of sol and gel ($0.58 \leq x \leq 1$). Prior to gelation ($x < 0.58$), the T_g of the material is equal to that of the sol. Fox and Loshaek[36] have shown that the T_g (K) of linear homologous polymer can be directly related to the number average molecular weight:

$$\frac{1}{T_g} = \frac{1}{T_g^\infty} + \frac{K_n}{M_n} \tag{16}$$

where T_g^∞ is the glass transition temperature of an infinitely long linear polymer and K_n is a constant parameter. By invoking the concept of equation of state, in which T_g is considered to be an index of the system state, DiBenedetto[37] has also derived a generalized expression for T_g that can be simplified to a form identical to the above equation for linear polymers. Equation (16) will be adopted for calculating the T_g of the sol fraction, in spite of the sol fraction consisting of both linear and branched molecules. Presumably for branched molecules, the constant, now designated K, in eq. (16) will change with the number of chain ends.[38] However, for simplicity, K will be treated as a constant.

The number average molecular weight can be related to the fractional conversion through stoichiometric considerations.[39]

$$\overline{M_n} = \frac{\text{total weight of the material}}{\text{number of molecules in the system}}$$

For the reaction of tetrafunctional amine and diepoxy molecules,

$$\overline{M_n} = \frac{M_A N_A + M_E N_E}{N_A + N_E - 2N_E x}$$

where the subscripts A and E represent the amine and epoxy molecules, respectively, M = molar molecular weight of each component, and N = number of moles of each component in the initial mixture. For the case of a stoichiometric ratio of the initial mixture ($N_E = 2N_A$),

$$\overline{M_n} = \frac{\overline{M_n}(0)}{1 - \frac{4}{3}x} \tag{17}$$

where $\overline{M_n}(0)$ is the number average molecular weight of the initial mixture.

Substituting $\overline{M_n}$ into eq. (16), the T_g of the ungelled material can be related to its chemical conversion:

$$\frac{1}{T_g} = \frac{1}{T_g^\infty} + \frac{K}{\overline{M_n}(0)} \left[1 - \frac{4}{3} x \right] \tag{18}$$

When $x = 0$, T_g^∞ can be expressed in terms of the initial glass transition temperature of the reactants, T_{g0}, and the constant parameter K from eq. (16), as

$$\frac{1}{T_g^\infty} = \frac{1}{T_{g0}} - \frac{K}{\overline{M_n}(0)} \tag{19}$$

Equation (18) in terms of T_{g0} and K becomes

$$\frac{1}{T_g} = \frac{1}{T_{g0}} - \frac{4K}{3\overline{M_n}(0)} x \tag{20}$$

The fit of the T_g vs. x data (Fig. 23) in the low conversion range ($x < 0.58$) suggests that the value of the parameter K in the above equation is a constant (with the best-fit value of 0.245).[7]

T_g after Gelation

For conversions greater than the critical gel point ($x > 0.58$), the reacting system can be considered to be a miscible binary mixture of sol and gel, and its T_g will be a combination of the T_g from each component. From a simple empirical rule of mixing,[40] the T_g of the binary mixture is given by

$$T_g = w_s T_{gs} + w_g T_{gg} \tag{21}$$

where w_s and w_g are the weight fractions of the sol and gel fractions, respectively, and T_{gs} and T_{gg} are the glass transition temperatures of the sol and gel fractions, respectively.

Miller and Macosko[34] have derived expressions for w_s as a function of the overall fractional conversion using a recursive probability method. For the current amine/epoxy system assuming a single rate constant, w_s is given as

$$w_s = w_A P^4 + w_E (x P^3 + 1 - x)^2 \tag{22a}$$

$$w_g = 1 - w_s \tag{22b}$$

$$P = \left(\frac{1}{x^2} - \frac{3}{4} \right)^{1/2} - \frac{1}{2} \tag{23}$$

where w_A and w_E are the weight fractions of the amine and epoxy molecules, respectively, and P is the probability of finding a finite chain when looking out from a randomly chosen amine molecule (see Appendix C).

The glass transition temperature of the sol fraction, T_{gs}, can be determined by eq. (16) using the number average molecular weight of the sol fraction, $\overline{M_{n,\text{sol}}}$, i.e.,

$$\frac{1}{T_{gs}} = \frac{1}{T_g^\infty} + \frac{K}{\overline{M_{n,\text{sol}}}} \tag{24}$$

$\overline{M_{n,\text{sol}}}$ can be calculated from the extent of reaction and the stoichiometric balance in the sol fraction [41]:

$$\overline{M_{n,\text{sol}}} = \frac{M_A + (2/r_{\text{sol}})M_E}{1 + 2/r_{sol} - 4x_{AS}} \tag{25}$$

where x_{AS} is the extent of reaction of amine in the sol fraction only, and r_{sol} is the stoichiometric balance between amino hydrogen and epoxy in the sol fraction. Both x_{AS} and r_{sol} can be related to x, the overall extent of reaction of the material as follows[41] (see Appendix C):

$$x_{AS} = \frac{x}{P}(xP^3 + 1 - x) \tag{26}$$

$$r_{\text{sol}} = \frac{x_{AS}}{x_{ES}} = \frac{P^4}{(xP^3 + 1 - x)^2} \tag{27}$$

where P is the same probability given as a function of x in eq. (23).

The glass transition temperature of the gel fraction, T_{gg}, can be evaluated from the expression relating T_g to $\overline{M_n}$ and crosslinking concentration, $[\rho_x]$, developed by Fox and Loshaek[36] for finite polymer chain with crosslinks:

$$T_{gg} = T_g^\infty - K/\overline{M_n} + K_x[\rho_x]$$

where T_g^∞ and K have the same meanings as for the linear (branched) systems, $[\rho_x]$ is the crosslink concentration, and K_x is a constant parameter.

The number average molecular weight of the gel fraction itself is infinite. Therefore, the above relationship reduces to

$$T_{gg} = T_g^\infty + K_x[\rho_x] \tag{28}$$

The recursive finite chain probability technique[34] has also been extended to calculate $[\rho_x]$ as a function of the extent of reaction. For the current system, if trifunctional and tetrafunctional crosslinking units are counted equivalently, the relationship for $[\rho_x]$ is given by (see Appendix C)

$$[\rho_x] = [\rho_3] + [\rho_4] \tag{29}$$

$$[\rho_3] = A_0 \times 4P(1 - P)^3 \tag{30a}$$

$$[\rho_4] = A_0 \times (1 - P)^4 \tag{30b}$$

where $[\rho_3]$ and $[\rho_4]$ are the concentrations of the trifunctional and tetrafunctional amine crosslinking units, respectively; A_0 is the initial amine concentration; and P has the same meaning and functional form of conversion as defined in eq. (23).

Parameters	Numerical values	
T_{g0}	$-4.9°C$	Experimental
$T_{g\infty}$	$178°C$	Experimental
T_g^∞	$61.25°C$	Calculated
$K_n (= K)$	0.2455	Calculated
$A_0 K_x$	116.75	Calculated
$\overline{M_n}(0)$	337.2 g/mol	Calculated
x_{gel}	0.58	Calculated

The parameter K_x can be determined from the maximum glass transition temperature of the fully cured material, $T_{g\infty}$. At $x = 1$, $T_g = T_{g\infty}$, $P = 0$, and $[\rho_x] = A_0$; therefore:

$$T_{g\infty} = T_g^\infty + K_x A_0$$

$$K_x = \frac{1}{A_0}(T_{g\infty} - T_g^\infty) \tag{31}$$

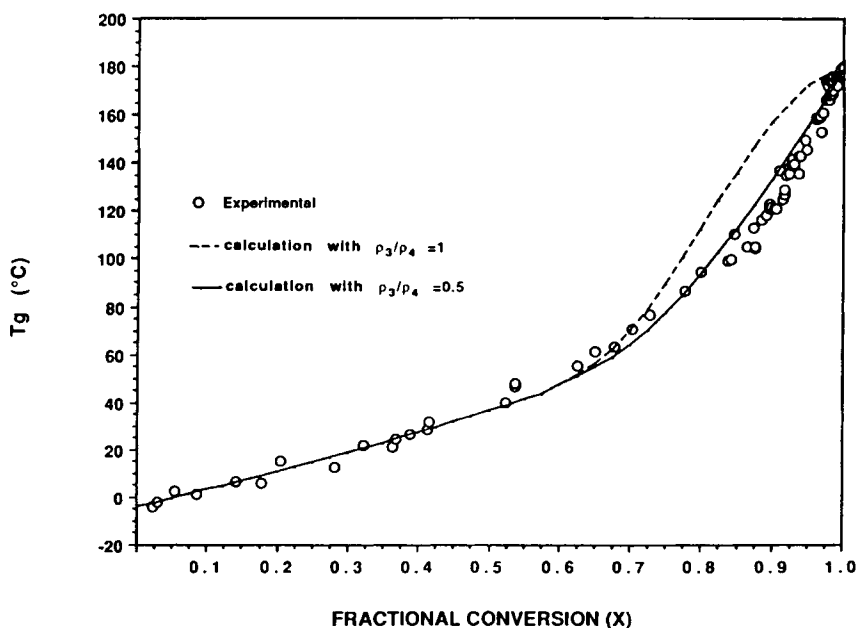**Tg VS. CONVERSION OF DER332/TMAB (1:1)**

Fig. 23. Calculation of T_g as a function of fractional conversion: (dashed line) weighting the amine crosslinking units of degree 3 and degree 4 equally; (solid line) weighting the amine crosslinking units of degree 3 as half of that of degree 4. Experimental data from Figure 7 (circles).

Equations (21)–(31) completely define the glass transition temperature of the material with conversion greater than that at the critical gel point.

T_g is calculated as a function of conversion using eq. (20) for conversions prior to the gel point, and eqs. (21)–(31), for conversions after the gel point. All physical parameters and constants for the system necessary for the calculation are listed in Table II. Figure 23 includes the calculation results as a dashed line over the entire conversion range compared with the experimental results (symbols). The correlation between the calculation and the experimental results after the gel point is not satisfactory. This poor correlation can be attributed to the inappropriate weighting factors to different crosslinking units (i.e., eq. (29) needs to be modified with different weighting factors for $[\rho_3]$ and $[\rho_4]$).

The sharp rise of T_g in the high conversion range has been attributed[10,32] to the higher effectiveness of higher-functional crosslinking units in raising the glass transition temperature. Figure 24 shows the relative concentration of trifunctional, $[\rho_3]$, and tetrafunctional, $[\rho_4]$, crosslinking units of the present amine/epoxy system calculated using eq. (29) over the entire conversion range. $[\rho_4]$ increases in the high conversion range at the expense of $[\rho_3]$. It is also noted that the shape of T_g vs. conversion resembles that of $[\rho_4]$ vs. conversion, which supports the hypothesis that T_g depends more strongly on $[\rho_4]$ than on $[\rho_3]$. Equation (29) is modified in order to take into account the effectiveness factor of the crosslinking units by replacing $[\rho_x]$ with $[\rho_x]_{\text{eff}}$, the effective crosslinking concentration. In evaluating $[\rho_x]_{\text{eff}}$, a trifunctional crosslinking unit is

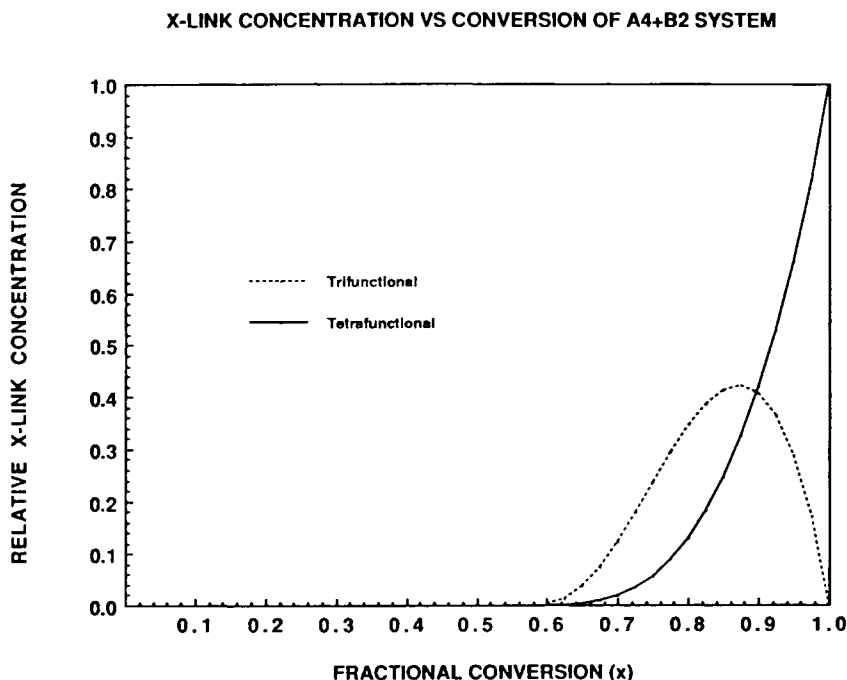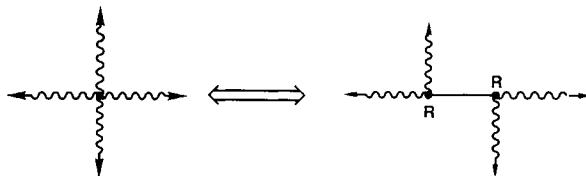**X-LINK CONCENTRATION VS CONVERSION OF A4+B2 SYSTEM**

Fig. 24. Relative concentrations of the amine crosslinking units of degree 3 and degree 4 vs. fractional conversion.

considered to be a half tetrafunctional unit since the latter is mechanically equivalent to two of the former in view of the following schematic:

where ∿∿► leads to infinite molecule, ———— represents a finite chain segment joining two trifunctional crosslinking units, and R is finite. Such a consideration has been invoked in other work relating the tensile modulus to the concentration of elastically effective strands in rubber networks.[42]

Therefore, the concentration of the effective crosslinking units is given by

$$[\rho_x]_{\text{eff}} = \tfrac{1}{2}[\rho_3] + [\rho_4], \tag{32}$$

where $[\rho_3]$ and $[\rho_4]$ are the same as given in eqs. (30a, b).

The modified calculation results of T_g vs. conversion using the effective crosslink concentration are included in Figure 23 as a solid line together with the actual experimental T_g vs. conversion data (symbols). The agreement is better than with the first calculation (comparing the solid line with the dashed line). The model provides a good correlation for the experimental data over the entire conversion range, although a few of the data at high conversion (between 85% and 95%) appear to lie below the calculation results. One reason to account for this discrepancy may be due to the DSC technique tending to underestimate the residual exotherm in the high conversion range, and, consequently, the conversion results estimated from the experimental exotherm can be higher than the actual conversion.

The effective crosslinking concentration, eq. (32), can be generalized for other functionalities, since a crosslinking unit of degree i (≥ 3) can be considered as mechanically equivalent to $(i - 2)$ crosslinking units of degree three.[42] Therefore, if a crosslinking unit of the highest degree in the system, m, is taken as an effective crosslink, then the weighting factor for each crosslinking unit of lower degrees ($3 \leq i < m$) is $(i - 2)/(m - 2)$. The total concentration of the effective crosslinking units can be calculated as

$$[\rho]_{\text{eff}} = \sum_{i=3}^{m} \frac{(i - 2)}{(m - 2)}[\rho_i]$$

where $[\rho_i]$ is the concentration of the crosslinking unit of degree i.

TTT Cure Diagram

The results of the previous sections can be conveniently summarized in the calculated isothermal TTT cure diagram shown in Figure 25, in which the glass transition temperature parameter is used as an index of the progress of cure. Fractional conversions (x) vs. time were calculated for $T_{\text{cure}} = -4$ to $200°C$. The results were converted into the corresponding values of T_g and are plotted

CALCULATED TTT DIAGRAM: ISO-Tg CONTOURS, MOLECULAR GELATION,
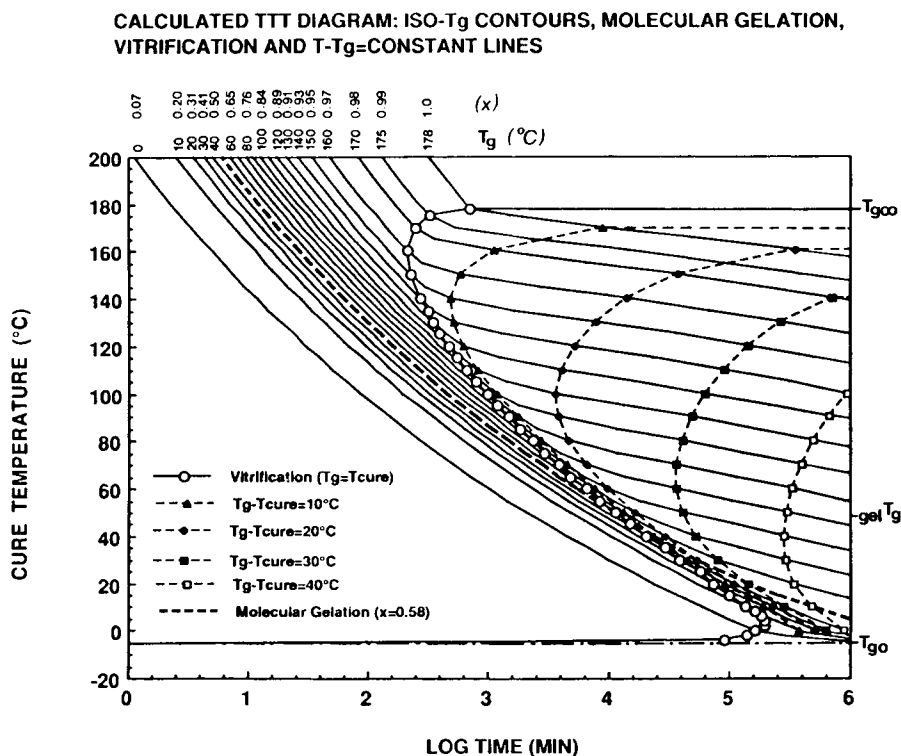VITRIFICATION AND T-Tg=CONSTANT LINES

Fig. 25. Calculated isothermal TTT cure diagram for the tetrafunctional aromatic diamine/
diepoxy system.

as a series of iso-T_g contours. The vitrification curve is constructed by joining
the vitrification points ($T_g = T_{cure}$) at all cure temperatures less than 178°C
($= T_{g\infty}$). The iso-T_g contours proceed beyond vitrification with a substantial
decrease in the slopes due to the effect of diffusion control. The transition
region after vitrification is also characterized by contours of ($T_g - T_{cure}$) = dif-
ferent constants, each of which provides the times for T_g to rise to a fixed value
above T_{cure}. The theoretical molecular gelation curve ($x = 0.58$), which cor-
responds to the iso-$T_g = 50.5$°C line, is also included in the diagram. The
molecular gelation curve intersects the vitrification curve at temperature
$_{gel}T_g$, which is equal to 50.5°C. The values of $_{gel}T_g$, T_{g0} ($= -4.9$°C), and
$T_{g\infty}(= 178$°C) are marked on the right-hand side of the diagram. The dia-
gram also includes the different conversions corresponding to the iso-T_g
contours.

The basic assumption in modeling the kinetics and the T_g vs. conversion
conversion was that the rate constants for the reactions of the epoxy with both
the primary and secondary amino hydrogens were equal. This assumed kinetics
has been tested further for nonisothermal curing conditions[43] and for off-stoi-
chiometric reactant ratios.[44] Spectroscopy (FTIR) is being used to determine
the ratio of the rate constants for the competing secondary amine/epoxy and
primary amine/epoxy reactions.[45] A more general theoretical justification for
the one-to-one T_g vs. conversion relationship is being developed on the basis

of the network being made up of trifunctional branching sites and the consequent insensitivity of the average molecular weight and crosslinking density to the ratio of rate constants of the competing amine/epoxy reactions.[46]

CONCLUSIONS

(1) A study of the isothermal cure behavior of the present tetrafunctional aromatic diamine-cured diglycidyl ether of bisphenol A epoxy system reveals that there is a unique one-to-one relationship between T_g and conversion independent of the cure temperature.

(2) T_g is used successfully as a direct measurement of chemical conversion. All the analyses are performed on the basis of the T_g data. When necessary, the T_g data are converted into a conversion basis through a fitting polynomial of the T_g vs. conversion relationship. The reasons for using T_g rather than the residual exotherm to measure conversion are the following: (a) T_g is more sensitive to the changes in chemical conversion, especially when the rate of chemical reaction is low, for example, in the high conversion range where the reactants are nearly depleted, and after vitrification, where the reaction is limited by diffusion of chain segments; and (b) T_g can be measured more accurately and displays significant changes over the entire range of conversion from the unreacted state up to full conversion, whereas the residual exotherm at high conversion is difficult to determine accurately due to the insensitivity of the DSC technique to low residual heat contents.

(3) Time-temperature shifts of the T_g vs. $\ln(t)$ data at different cure temperatures to form a master curve at a reference cure temperature (140°C in this analysis), according to the assumption that the reaction is purely kinetically controlled, yield an activation energy for the reaction equal to 15.2 kcal/mol. The single activation energy suggests that only one overall reaction mechanism dominates the curing reaction of the present epoxy/amine system. The isothermal vitrification points at all cure temperatures lie on the master curve, which indicates that the reaction prior to vitrification is only kinetically controlled. Deviations from the master curve occur shortly after vitrification for cure temperatures less than $T_{g\infty}$, revealing the onset of diffusion control.

(4) The kinetically controlled master curve, together with the calculated activation energy, is used as a basis for a simple calculation for the vitrification curve and iso-T_g contours in the TTT cure diagram. The basic assumptions of the calculation are that T_g is related to conversion in a one-to-one fashion and that a kinetically controlled reaction dominates up to vitrification. Both assumptions are satisfied by the current amine/epoxy system.

(5) The kinetically controlled master curve of T_g vs. time at 140°C is converted into a conversion basis and analyzed with an autocatalytic kinetic rate expression, which is based on the reactions between epoxide groups and amino hydrogens being catalyzed by the hydroxyl groups generated during the reactions. The results shows that the chemical kinetics of
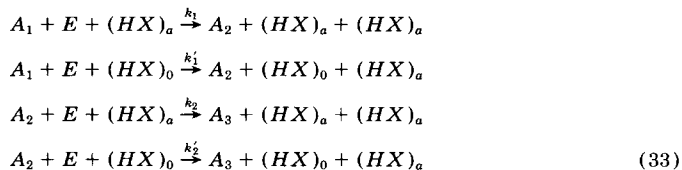
the reaction can be described by the autocatalytic rate law over the entire conversion range.

(6) The satisfactory correlation of the autocatalytic kinetic expression using a single rate constant with the experimental results, together with the unique one-to-one relationship between T_g and conversion, suggests that all amino hydrogens react with equal reactivity.

(7) The effect of diffusion control can be incorporated into the reaction kinetics by modifying the overall rate constant. During the course of isothermal curing, both in the kinetically and diffusion-controlled regimes, the overall rate constant is assumed to be a combination, in parallel, of the chemical rate constant and the diffusion rate constant. The temperature dependence of the kinetically controlled rate constant is given by the Arrhenius-type expression, whereas that of the diffusion-controlled rate constant is assumed to be given by a modified form of the WLF equation. Calculations using such modified rate constants provide good correlation with the experimental results at all cure temperatures. If valid, this would suggest that the constants in the WLF equation are independent of temperature and conversion.

(8) A theoretical model is presented to provide a fundamental molecular basis to support the premise that T_g is a one-to-one function of chemical conversion. The model assumes that there is only one rate constant for bond formation. Prior to gelation, only finite molecules are present in the system and the T_g of the material varies with the increasing number average molecular weight. After gelation, however, the system consists of both sol and gel fractions, both contributing to the increase in the T_g of the material. The T_g of the sol is a function of the number average molecular weight in the sol fraction only, whereas the T_g of the gel is a function of crosslink concentration, depending more strongly on higher functional crosslinking units than on the lower ones. In the calculation model for this system, tetrafunctional crosslinking units are found to be twice as effective in raising the T_g of the gel function as trifunctional crosslinking units. This relationship between the degree of crosslink and its effect on raising T_g can be generalized for higher functionalities: A crosslink of degree i is mechanically equivalent to $(i-2)$ crosslinks of degree three.

(9) The concept of the TTT isothermal cure diagram has been extended to include characterization of the progress of the reaction beyond vitrification.

APPENDIX A

Autocatalyzed Reaction Kinetics[17]

$$A_1 + E + (HX)_a \xrightarrow{k_1} A_2 + (HX)_a + (HX)_a$$

$$A_1 + E + (HX)_0 \xrightarrow{k_1'} A_2 + (HX)_0 + (HX)_a$$

$$A_2 + E + (HX)_a \xrightarrow{k_2} A_3 + (HX)_a + (HX)_a$$

$$A_2 + E + (HX)_0 \xrightarrow{k_2'} A_3 + (HX)_0 + (HX)_a \qquad (33)$$

(See regular text for the species represented by each symbol.)

Let e, a_1, and a_2 be the molar concentrations at time t of E, A_1, and A_2, respectively; e_0 and a_0, the initial concentrations of E and A_1; and c_0, the initial concentration of $(HX)_0$. The concentration of $(HX)_a$ at time t is the same as the epoxide concentration that has reacted, i.e., $[HX]_a = e_0 - e = xe_0$, where x is the fractional epoxide conversion. The rate of epoxide consumption is given by

$$-\frac{de}{dt} = k_1 a_1 e (e_0 - e) + k_1' a_1 e c_0 + k_2 a_2 e (e_0 - e) + k_2' a_2 e c_0$$

$$\frac{dx}{dt} = k_1 a_1 (1 - x)(xe_0) + k_1' a_1 (1 - x) c_0 + k_2 a_2 (1 - x)(xe_0) + k_2' a_2 (1 - x) c_0$$

$$\frac{dx}{dt} = (1 - x)[a_1(k_1(xe_0) + k_1'c_0) + a_2(k_2(xe_0) + k_2'c_0)]$$

$$\frac{dx}{dt} = (1 - x)(k_1 e_0 x + k_1' c_0)(a_1 + r_k a_2) \tag{34}$$

where $r_k = k_2/k_1 = k_2'/k_1'$ is the reactivity ratio of the secondary amine group to the primary amine group. Assuming that all amino hydrogen atoms are equally reactive, the primary amine group, A_1, will be twice as reactive as the secondary amine group, A_2, since the former contain twice as many reactive hydrogens as the latter. Therefore,

$$\frac{k_2}{k_1} = \frac{k_2'}{k_1'} = \frac{1}{2}$$

According to the above definition, k_1 is the rate constant of the reaction between the amine and epoxy groups. If the rate constant is defined, instead, in terms of the reaction between an aminohydrogen atom and an epoxy group, k_1^*, then the value of $k_1^* = k_1/2$, and the ratio k_2/k_1^* is equal to 1 for the ideal case of equal reactivity of all amino hydrogens. With either definition of the rate constant, the above rate expression can be simplified to

$$\frac{dx}{dt} = (1 - x)(k_1 e_0 x + k_1' c_0)\left(a_1 + \frac{a_2}{2}\right).$$

From the balance of amino hydrogens at time t,

$$2a_1 + a_2 = 2a_0 - xe_0$$

$$a_1 + \frac{a_2}{2} = a_0 - \frac{xe_0}{2}$$

therefore,

$$\frac{dx}{dt} = (1 - x)(k_1 e_0 x + k_1' c_0)\left(a_0 - \frac{xe_0}{2}\right)$$

$$= \frac{k_1 e_0^2}{2}(1 - x)\left(x + \frac{k_1' c_0}{k_1 e_0}\right)\left(\frac{2a_0}{e_0} - x\right)$$

$$= k(1 - x)(x + B)(r - x)$$

where $k = (k_1 e_0^2)/2$, $B = (k_1' c_0)/(k_1 e_0)$, and $r = (2a_0)/e_0$ is the stoichiometric ratio of amino hydrogen to epoxy. For an initial stoichiometric mixture, $r = 1$, the rate expression reduces to eq. (8):

$$\frac{dx}{dt} = k(1 - x)^2(x + B) \tag{8}$$

APPENDIX B

Effect of Varying k_2/k_1 on the Determined Kinetics

The autocatalytic kinetic model without assuming equal reactivity of primary amino and secondary amino hydrogens is given by eq. (34) in Appendix A:

$$\frac{dx}{dt} = k_1 e_0 (1 - x) \left(x + \frac{k_1' c_0}{k_1 e_0} \right) (a_1 + r_k a_2),$$

where $r_k = k_2/k_1 = k_2'/k_1'$.

From the balance of amino hydrogens, $a_2 = 2a_0 - xe_0 - 2a_1$, the above equation becomes

$$\frac{dx}{dt} = \frac{k_1 e_0^2}{2} (1 - x) \left(x + \frac{k_1' c_0}{k_1 e_0} \right) \left(2 \frac{a_1}{e_0} (1 - 2r_k) + 2r_k (r - x) \right)$$

$$\frac{dx}{dt} = k (1 - x)(x + B)(y(1 - 2r_k) + 2r_k(r - x)), \tag{35}$$

where $k = (k_1 e_0^2)/2$, $B = (k_1' c_0)/(k_1 e_0)$, and $r = (2a_0)/e_0$ as defined in Appendix A, and $y = 2a_1/e_0$ is the normalized primary amine group concentration.

The rate of change of the primary amine group concentration, a_1, can be determined from the autocatalytic reaction scheme:

$$-\frac{da_1}{dt} = k_1 a_1 e (e_0 - e) + k_1' a_1 e c_0$$

$$\frac{d\,2a_1/e_0}{dt} = -k_1 e_0^2 (1 - x) \left(x + \frac{k_1' c_0}{k_1 e_0} \right) \frac{2a_1}{e_0}$$

$$\frac{dy}{dt} = -2k(1 - x)(x + B)y, \tag{36}$$

where k, B, and y are as previously defined.

The influence of varying the reactivity ratio, r_k, on the calculated kinetics can be examined by solving the two coupled ordinary differential equations (35) and (36) using the kinetic parameters k and B determined for the case of equal reactivity (i.e., $k = 6.679E - 2$ at 140°C and $B = 5.548E - 2$) for the present analysis. The initial conditions for the variables x and y in these equations are $x(t = 0) = 0$ and $y(t = 0) = 2a_0/e_0 = 1$ for a stoichiometric ratio reaction. The two coupled differential equations are solved numerically using the fourth-order Runge–Kutta method for different values of r_k ($r_k = 0.05, 0.1, 0.25, 0.5, 0.75,$ and 1.0). The integration results at 140°C in terms of x vs. log(time) and T_g vs. log(time) are summarized in Figures 26 and 27, respectively.

These calculations show the sensitivity of the kinetic model at fixed constant parameters (k and B) to the perturbation in the reactivity ratio (r_k). The results show that increasing r_k results in an increase in the overall rate of reaction, which reflects a faster consumption rate of epoxy groups (for the case of higher r_k) by secondary amines. For the cases of very low r_k (e.g., $r_k < 0.1$), the epoxy conversion vs. time curves exhibit a two-stage reaction behavior. The first stage involves primarily the reaction of primary amines with epoxy groups; the reaction due to secondary amines, which accounts for the second stage, is significant only after all primary amines are depleted.

The kinetics of the overall reaction is not highly sensitive, however, to a small variation in the reactivity ratio for the cases of small to no substitution effect (i.e., r_k close to 0.5). Figure 28 shows the calculated T_g vs. log(time) at 140°C for the cases of $r_k = 0.3$–0.5, together with the experimental T_g of the kinetically controlled master curve at 140°C. The analysis shows that the present experimental data can be correlated with the values of r_k between 0.4 and 0.5.
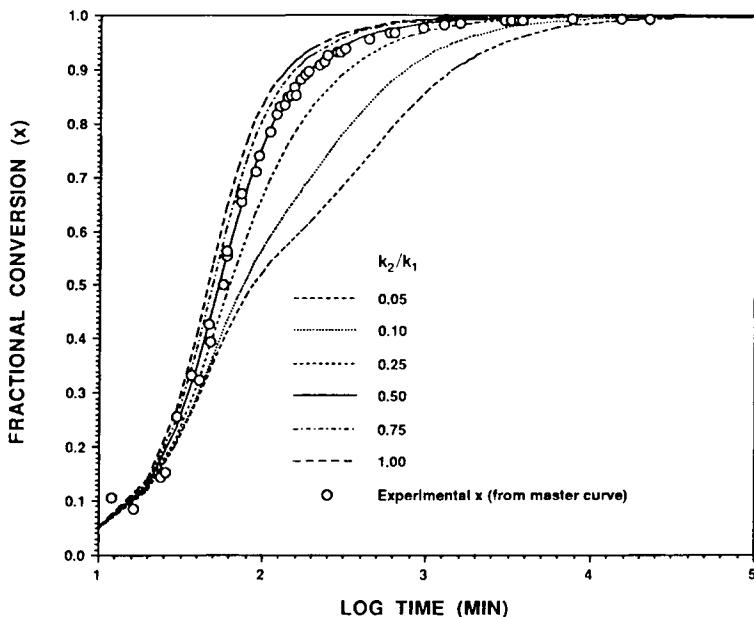
CALCULATED X VS. LOG(TIME) AT 140°C FOR DIFFERENT REACTIVITY RATIOS (k2/k1)

Fig. 26. Calculated x vs. log(time) at 140°C for different reactivity ratios (curves). Experimental data from the kinetically controlled master curve at 140°C (O). Note the two-stage reaction behavior for the cases of very low reactivity ratios (e.g., 0.05 and 0.10).
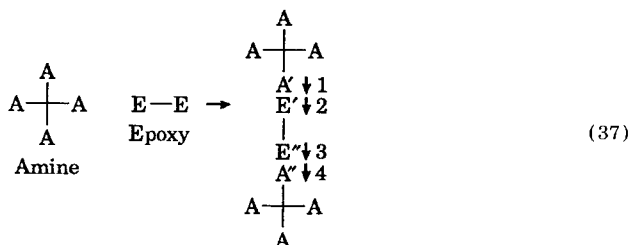
In future work, the reactivity ratio should be determined independently using spectroscopic techniques such as FTIR to monitor the rates of disappearance of both epoxy, and primary and secondary amine groups, which can provide complementary information on the relative reactivities of the primary vs. secondary amine groups. The reaction rate constant k and the parameter B can then be evaluated by fitting the conversion data to the kinetic rate eqs. (35) and (36).

APPENDIX C

Recursive Probability Method

Miller and co-workers[34,39,41] have presented a recursive probability approach for treating nonlinear network formation. Employing the elementary law of conditional probability and the recursive nature of the polymerization process, several important properties can be calculated. Relevant calculations (used in the present model study of T_g vs. conversion) for the reaction of the type A_4 + $2B_2$ (e.g., tetrafunctional amine + difunctional epoxy) are summarized in this section.

The reaction between tetrafunctional amine and difunctional epoxy can be schematically represented by the following diagram:

$$
\begin{array}{cccc}
& & & A \\
& & & A\!-\!\!\!+\!\!\!-A \\
& A & & A'\ \downarrow 1 \\
A\!-\!\!\!+\!\!\!-A & E\!-\!E & \rightarrow & E'\ \downarrow 2 \\
& A & \text{Epoxy} & | \\
& \text{Amine} & & E''\ \downarrow 3 \\
& & & A''\ \downarrow 4 \\
& & & A\!-\!\!\!+\!\!\!-A \\
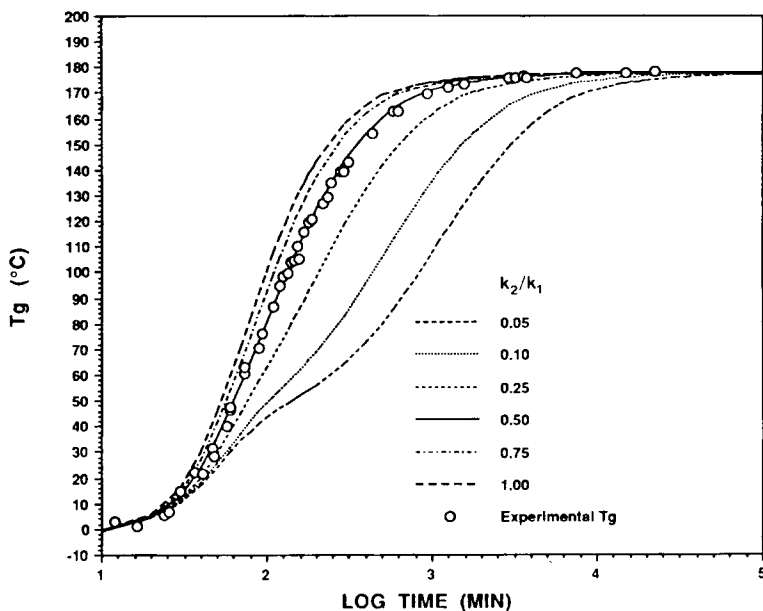& & & A
\end{array}
\qquad (37)
$$

CALCULATED Tg VS. LOG(TIME) AT 140°C FOR DIFFERENT REACTIVITY RATIOS (k2/k1)

Fig. 27. Calculated T_g vs. log(time) at 140°C for different reactivity ratios (curves). Experimental data from the kinetically controlled master curve at 140°C (O).

In the following calculations, the usual conditions for Flory's ideal network are assumed:

(1) all functional groups of the same type are equally reactive;

(2) all groups react independently of one another;

(3) no intramolecular reactions occur.

Probability of a Finite Chain, P

Let $P(F_A^{out})$ be the probability of finding a finite chain when looking out from a randomly chosen amine molecule. Consider the schematic (37); looking out of A' along $\overset{1}{\rightarrow}$, $P(F_A^{out})$ can be calculated from the law of total probability:

$$P(F_A^{out}) = P(F_A^{out} | A \text{ reacts})P(A \text{ reacts}) + P(F_A^{out} | A \text{ does not react})P(A \text{ does not react})$$

$$P(F_A^{out}) = x_A P(F_E^{in}) + 1 - x_A, \tag{38}$$

where $P(F_E^{in})$ is the probability of the event that $\overset{2}{\rightarrow}$ is the start of a finite chain, and x_A is the fractional conversion of the amine. The probability of E' looking along $\overset{2}{\rightarrow}$ leading to a finite chain is the same as E'' looking along $\overset{3}{\rightarrow}$. Therefore,

$$P(F_E^{in}) = P(F_A^{out}). \tag{39}$$

Similarly, from the law of total probability,

WISANRAKKIT AND GILLHAM

CALCULATED Tg VS. LOG TIME AT 140°C FOR
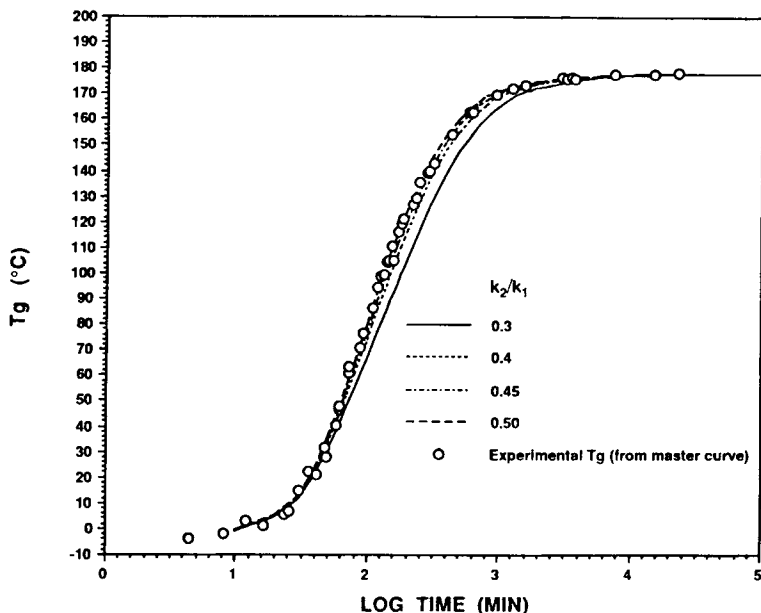THE CASES OF WEAK TO NO SUBSTITUTION EFFECT

Fig. 28. Calculated T_g vs. log(time) at 140°C for the cases of weak to no substitution effect ($0.3 \leq k_2/k_1 \leq 0.5$). Experimental data from the kinetically controlled master curve at 140°C (O). Note the value of k_2/k_1 is therefore between 0.4 and 0.5.

$$P(F_E^{out}) = x_B P(F_A^{in}) + 1 - x_B$$
$$= rx_A P(F_A^{in}) + 1 - rx_A, \tag{40}$$

where r is the stoichiometric ratio of amino hydrogen to epoxy ($x_B = rx_A$). Finally, for A'' to lead to a finite chain, all of the other arms of the amine molecule must be finite.

$$P(F_A^{in}) = [P(F_A^{out})]^3. \tag{41}$$

Combining eqs. (38)–(41) yields

$$rx^2 P(F_A^{out})^3 - P(F_A^{out}) - rx^2 + 1 = 0. \tag{42}$$

The solution of eq. (42) before gelation is 1, implying that all chains are finite. In the postgel stages, a unique nonunity solution is given by

$$P(F_A^{out}) = \left(\frac{1}{rx^2} - \frac{3}{4}\right)^{1/2} - \frac{1}{2}. \tag{43}$$

For the case of stoichiometric mixture, $r = 1$, eq. (43) reduces to eq. (23) with $P(F_A^{out})$ simply written as P:

$$P = \left(\frac{1}{x^2} - \frac{3}{4}\right)^{1/2} - \frac{1}{2}. \tag{23}$$

Weight Fraction of Solubles, w_s

A randomly chosen amine molecule will be part of the sol fraction if all of its arms lead out to finite chains. The probability of such an event is given by

$$w_{A,sol} = P(F_A^{out})^4. \tag{44}$$

Similarly, the probability that an epoxide molecule will be part of the sol is

$$w_{E,sol} = P(F_E^{out})^2. \tag{45}$$

Weighting each species by its mass fraction in the mixture, the result is the total weight fraction of the sol:

$$w_s = w_A P(F_A^{out})^4 + w_E P(F_E^{out})^2$$

$$w_s = w_A P^4 + w_E (xP^3 + 1 - x)^2 \tag{22a}$$

$$w_g = 1 - w_s \tag{22b}$$

Fractional Conversion in the Sol Fraction, x_s

The extent of reaction of the amine in the sol fraction is the probability that a randomly chosen amine molecule, looking out, has reacted, given that it is also part of a finite chain, i.e.,

$$x_{A,sol} = P(A \text{ reacts} | F_A^{out}). \tag{46}$$

From the definition of conditional probability,

$$x_{AS} = \frac{P(F_A^{out} | A \text{ reacts}) P(A \text{ reacts})}{P(F_A^{out})}$$

$$= \frac{P(F_E^{in}) P(A \text{ reacts})}{P(F_A^{out})} \tag{47}$$

$$x_{AS} = \frac{x}{P} (xP^3 + 1 - x). \tag{26}$$

Similarly, the extent of reaction of the epoxy group in the sol fraction is

$$x_{ES} = \frac{P(F_A^{in}) x_E}{P(F_E^{out})} = \frac{P^3 x}{xP^3 + 1 - x}. \tag{48}$$

Number Average Molecular Weight of the Sol Fraction, $\overline{M}_{n,sol}$

Let N_{AS} and N_{ES} be the number of moles of amine and epoxy in the sol fraction, respectively, when the total conversion of the material is x ($= x_A = x_B$):

$$N_{AS,reacted} = N_{AS} x_{AS}$$

$$N_{ES,reacted} = N_{ES} x_{ES}.$$

Since one epoxide group reacts with one amino hydrogen,

$$4N_{AS,reacted} = 2N_{ES,reacted}$$

$$4N_{AS}x_{AS} = 2N_{ES}x_{ES}.$$

The stoichiometric balance in the sol fraction, r_{sol}, is defined as

$$r_{sol} \equiv \frac{x_{AS}}{x_{ES}} = \frac{2N_{AS}}{N_{ES}}. \tag{49}$$

Therefore,

$$r_{sol} \equiv \frac{x_{AS}}{x_{ES}} = \frac{P^4}{(xP^3 + 1 - x)^2} \tag{27}$$

$$\overline{M_{n,sol}} = \frac{M_A N_{AS} + M_E N_{ES}}{N_{AS} + N_{ES} - 4N_{AS}x_{AS}}$$

$$\overline{M_{n,sol}} = \frac{M_A + M_E(N_{ES}/N_{AS})}{1 + (N_{ES}/N_{AS}) - 4x_{AS}} \tag{50}$$

$$\overline{M_{n,sol}} = \frac{M_A + \dfrac{2}{r_{sol}} M_E}{1 + \dfrac{2}{r_{sol}} - 4x_{AS}}. \tag{25}$$

Crosslink Concentration, $[\rho_x]$

An amine molecule (A_4) chosen at random will be an effective crosslinking unit if at least three of its four arms lead out to the infinite molecule. The probability that the amine will be a crosslink of degree 4 (i.e., all of the fours arms are connected to the inifinite network) is given by

$$P(X_4) = [1 - P(F_A^{out})]^4 = (1 - P)^4, \tag{51}$$

and that it will be a crosslink of degree 3 (i.e., if exactly three of its four arms are infinite) is given by

$$P(X_3) = \binom{4}{3} P(F_A^{out})[1 - P(F_A^{out})]^3 = 4P(1 - P)^3. \tag{52}$$

The concentration of each type of the amine crosslinking units ($[\rho_3]$ or $[\rho_4]$) is found from the initial amine concentration A_0 times the corresponding probability:

$$[\rho_3] = A_0 \times P(X_3) = A_0 \times 4P(1 - P)^3 \tag{30a}$$

$$[\rho_4] = A_0 \times P(X_4) = A_0 \times (1 - P)^4. \tag{30b}$$

References

1. J. K. Gillham, in *Developments in Polymer Characterisation-3*, J. V. Dawkins, Ed., Applied Science, London, 1982, Chap. 5.
2. J. K. Gillham, *Polym. Eng. Sci.*, **19**, 670 (1979); **26**(20), 1429 (1986).
3. J. B. Enns and J. K. Gillham, in *Polymer Characterization*, Am. Chem. Soc. Advances in Chemistry Series No. 203, C. D. Craver, Ed., Am. Chem. Soc., Washington, DC, 1983, pp. 27–63.
4. J. B. Enns and J. K. Gillham, *J. Appl. Polym. Sci.*, **28**, 2567 (1983).

5. I. Mita and K. Horie, *J. Macromol. Sci. Rev. Macromol. Chem. Phys.*, **C27**(1), 91 (1987).

6. G. Wisanrakkit and J. K. Gillham, *J. Coat. Technol.*, **62**(783), 35(1990).

7. G. Wisanrakkit, Ph.D. Dissertation, Department of Chemical Engineering, Princeton University 1990.

8. R. B. Prime in *Thermal Characterization of Polymeric Materials*, E. A. Turi, Ed., Academic, New York, 1981, p. 435.

9. I.-C. Choy and D. J. Plazek, *J. Polym. Sci. Polym. Phys. Ed.*, **24**, 1303 (1986).

10. K. P. Pang and J. K. Gillham, *J. Appl. Polym. Sci.*, **37**, 1969 (1989); **39**, 909 (1990).

11. M. A. Acitelli, R. B. Prime, and E. Sacher, *Polymer*, **12**, 333 (1971).

12. S. Lunak, J. Vladyka, and K. Dusek, *Polymer*, **19**, 931 (1978).

13. J. M. Barton, *Br. Polym. J.*, **11**, 115 (1979).

14. S. Gan, J. K. Gillham, and R. B. Prime, *J. Apply. Polym. Sci.*, **37**, 803 (1989).

15. G. Wisanrakkit and J. K. Gillham, *Am. Chem. Soc. Prepr. Div. Polym. Mater. Sci. Eng.*, **59**, 969 (1988); also *Soc. Plast. Eng. ANTEC '89*, 1523 (1989).

16. I. T. Smith, *Polymer*, **2**, 95 (1961).

17. K. Horie, H. Hiura, M. Sawada, I. Mita, and H. Kambe, *J. Polym. Sci. A-1*, **8**, 1357 (1970).

18. J. Charlesworth, *J. Polym. Sci. Polym. Chem. Ed.*, **18**, 621 (1980).

19. C. R. Riccardi and R. J. J. Williams, *J. Appl. Polym. Sci.*, **32**, 3445 (1986).

20. C. S. P. Sung, E. Pyun, and H.-L. Sun, *Macromolecules*, **19**, 2922 (1986).

21. S. Lunak and K. Dusek, *J. Polym. Sci. Polym. Symp.*, **53**, 45 (1976).

22. S. Sourour and M. R. Kamal, *Thermochim. Acta*, **14**, 41 (1976).

23. A. Dutta and M. E. Ryan, *J. Appl. Polym. Sci.*, **24**, 635 (1979).

24. C. C. Riccardi, H. E. Adabbo, and R. J. J. Williams, *J. Appl. Polym. Sci.*, **29**, 2481 (1984).

25. M. R. Keenan, *J. Appl. Polym. Sci.*, **33**, 1725 (1987).

26. I. Havlicek and K. Dusek, in *Crosslinked Epoxies*, B. Sedlacek and J. Kahovec, Eds., Walter de Gruyter, New York, 1987, pp. 417–424.

27. E. Rabinowitch, *Trans. Faraday Soc.*, **33**, 1225 (1937).

28. M. L. Williams, R. F. Landel, and J. D. Ferry, *J. Am. Chem. Soc.*, **77**, 3701 (1955).

29. D. H. Kaelble, *Computer Aided Design and Manufacture*, Dekker, New York, 1985, chap. 4, pp. 113–148.

30. K. C. Rusch, *J. Macromol. Sci., Phys.* **B2**(2), 179 (1968).

31. M. Gordon and W. Simpson, *Polymer*, **2**(4), 383 (1961).

32. A. Hale, C. W. Macosko, and H. E. Bair, *Soc. Plast. Eng. ANTEC '87*, 1116 (1987).

33. P. J. Flory, *Principles of Polymer Chemistry*, Cornell University Press, Ithaca, NY, 1953.

34. D. R. Miller and C. W. Macosko, *Macromolecules*, **9**(2), 206 (1976).

35. M. T. Aronhime, and J. K. Gillham, *J. Coat. Technol.*, **56**(718), 35 (1984).

36. T. G. Fox and S. Loshaek, *J. Polym. Sci.*, **15**, 371 (1955).

37. A. T. DiBenedetto, *J. Polym. Sci. Polym. Phys., ed.*, **25**, 1949 (1987).

38. P. Meare, *Trans. Faraday Soc.*, **53**, 31 (1957).

39. C. W. Macosko and D. R. Miller, *Macromolecules* **9**(2), 199 (1976).

40. J. R. Fried, in *Developments in Polymer Characterisation—4*, J. V. Dawkins, Ed., Applied Science, London, (1983), Chap. 2, p. 47.

41. D. R. Miller, E. M. Valles, and C. W. Macosko, *Polym. Eng. Sci.*, **19**(4), 272 (1978).

42. N. R. Langley and K. E. Polmanteer, *J. Polym. Sci. Polym. Phys. Ed.*, **12**, 1023 (1974).

43. G. Wisanrakkit and J. K. Gillham, *J. Appl. Polym. Sci.*, to appear; also *Polym. Prepr. Am. Chem. Soc. Div. Polym. Chem.*, **31**(1), (1990).

44. S. L. Simon G. Wisanrakkit, and J. K. Gillham, *J. Appl. Polym. Sci.*, to appear; also *Am. Chem. Soc. Prepr. Div. Polym. Mater. Sci. Eng.*, **61**, 799 (1989).

45. X. Wang and J. K. Gillham, *J. Appl. Polym. Sci.*, to appear; also *Am. Chem. Soc. Prepr. Div. Polym. Mater. Sci. Eng.*, **63**, 505 (1990).

46. X. Wang and J. K. Gillham, *J. Appl. Polym. Sci.*, to appear; also *Am. Chem. Soc. Prepr. Div. Polym. Mater. Sci. Eng.*, **63**, 753 (1990).